Phase Diagrams for Asphaltene and Asphaltene-Rich Hydrocarbons + Polystyrene + Toluene mixtures

by

Sourav Chowdhury

A thesis submitted in partial fulfillment of the requirements for the degree of

Master of Science

in

CHEMICAL ENGINEERING

Department of Chemical and Materials Engineering
University of Alberta

Abstract

Heavy oils are nano-colloids comprising a continuous maltene-rich liquid phase and a nano-dispersed asphaltene-rich phase separable by filtration that are macroscopically homogeneous. The asphaltene-rich phase can aggregate and deposit, causing technological risk and process operation challenges for the hydrocarbon production, transport and refining industries. When non-adsorbing polymers are added to nano-colloids two stable macroscopic fluid phases arise due to depletion flocculation. One phase is rich in polymer (polystyrene in this case) and the other phase is rich in nano-colloid (asphaltenes in this case). In the present study the phase behavior of mixtures comprising chemically separated pentane asphaltenes + toluene + atactic polystyrene (400,000 AMU) is revisited and the phase behavior of Athabasca bitumen (naturally-occurring hydrocarbon resource with 18.6 wt.% pentane asphaltenes) + toluene + atactic polystyrene (400,000 AMU) mixtures is explored. For both mixtures critical points associated with depletion flocculation and depletion re-stabilization are identified on closed loop two-phase to one-phase boundaries. The experimental methods, phase boundaries, tie lines and fluid-fluid critical points are presented and discussed. We show that X-ray transmission is more robust than acoustic transmission for the identification of two-phase to one-phase boundaries and critical points in these mixtures. The outcomes of this work are expected to improve the understanding of asphaltene behaviours in current production, transport, and refining processes, and may lead to the development of new low-environmental impact de-asphalting processes for heavy oils.

Acknowledgements

First and foremost, I would like to express my deepest gratitude to my supervisor, Dr. John M. Shaw, for his supervision, insight, advice, guidance and encouragements throughout my graduate studies. This work could not have been completed without those encouragements.

Special thanks to our lab manager, Ms Mildred Becerra for her help with experiments in the lab. Her advice and presence in the lab were invaluable.

I am deeply indebted to my parents and relatives for their support, encouragement, and guidance all over my life.

Finally, I acknowledge, with thanks, financial support from the sponsors of NSERC Industrial Research Chair in Petroleum Thermodynamics: Natural Sciences and Engineering Research Council of Canada (NSERC), Alberta Innovates - Energy and Environmental Solutions, British Petroleum Canada Energy Corporation, ConocoPhillips Canada Resource Corporation, Nexen Energy ULC, Shell Canada Ltd., Total E&P Canada Ltd., Virtual Materials Group Incorporated.

Table of Contents

List of Figures:

List of Tables:

Nomenclature

R_g	radius of gyration of polymer
a	colloidal particle radius
γ	the fraction of asphaltene colloidal particles causing phase separation
δ	depletion layer thickness around colloidal particle
R	volume fraction of the upper phase
MW	molar mass of polymer
G	colloid gas like phase
L	colloid liquid like phase
C	colloid rich phase
G+C	colloid gas-particle region
G+L	colloid gas-liquid region
G+L+C	colloid gas-liquid-particle region
I_o	source intensity
I	transmitted intensity
λ	wavelength
ρ	density of sample mixture
μ	mass attenuation coefficient

w_i	weight fraction of the i^{th} component
FVT	free volume theory
GFVT	generalized free volume theory
ρ_r	density of retentate
ρ_o	density of asphaltene free retentate
ρ_{ar}	density of asphaltene in the retentate
m_o	mass fraction of asphaltene free retentate
m_{ar}	mass fraction of asphaltene in the retentate
$\mathrm{V_{ar}}$	volume fraction of asphaltene in the retentate
V_{aR}	Volume fraction of asphaltene in mixtures of retentate + toluene + polystyrene

Chapter 1: Introduction

Mixtures of nanoparticles + solvents + polymers arise in diverse industries as process streams or products [1]. Their properties and phase behaviour have attracted considerable practical and fundamental interest. Polymers that sorb on individual nanoparticle surfaces can be used to stabilize dispersions [2]. Polymers that sorb on multiple nanoparticles simultaneously cause nanoparticles to flock (bridging flocculation), which facilitates nanoparticle settling and separation [2]. With non-adsorbing polymers a polymer free layer, called the depletion layer, arises around particles. When depletion layers, with thickness δ, overlap as shown in Figure 1.1 colloidal particles aggregate because of an imbalance in osmotic pressure. While the kinetics are slow, over time this process leads to bulk phase separation. One phase is colloid rich and the other phase is polymer rich. While both phases are liquid continuous, the colloid rich phase is referred to as a colloid liquid, and the polymer-rich phase is referred to as a colloid gas. This separation mechanism, the subject of the present study, is called depletion flocculation. Phase separation by depletion flocculation has been observed in diverse contexts [3 4 5]. The physics and chemistry associated with this phase separation mechanism is understood conceptually [6 7] and there are both colloid specific models of varying complexity [8 9 10] and equation of state approaches [11] available for the correlation and interpretation of experimentally observed phase behaviors.

Asphaltenes, a polydispersed and nanoaggregated, supra molecular fraction of crude oil are thought to be responsible for significant problems during production, transport and refining of crude oils and crude oil fractions because they have a tendency to agglomerate and then deposit in response to changes in pressure and temperature [12], and global composition. The colloidal nature of asphaltenes leads to their phase separation in the presence of non-adsorbing polymer due to

depletion flocculation [13 14]. This fraction, a frequent subject of laboratory studies, is separated from hydrocarbon resources or resource fractions by precipitation with n-pentane or n-heptane according to ASTM D4055 or ASTM D6560 methods followed by filtration and washing steps. Regrettably, chemically separated asphaltenes are poor mimics for the naturally aggregated asphaltene-rich materials in crude oils and crude oil fractions. Their size, phase behaviour, and chemical composition all differ [15 16 17]. These differences underscore the importance of investigating depletion flocculation driven phase behaviors of naturally occurring hydrocarbon mixtures that include nanostructured asphaltene-rich species.

In this work, the phase behavior of mixtures of asphaltene-rich, naturally-occurring hydrocarbons (Athabasca bitumen and nanofiltered subfractions) + polystyrene + toluene are investigated. The observed phase behaviours are then compared to analogous mixtures comprising chemically separated asphaltenes. Implications for the findings, including improved approaches for asphaltene deposition modeling and deasphalting process design, are identified and discussed. Further two experimental phase boundary detection techniques, namely Acoustic transmission and X-ray transmission tomography, are compared. Sensitivity limitations of the acoustic transmission technique are identified. This thesis comprises five chapters. Following the introduction, Chapter 2 comprises a brief literature review on colloidal nature of asphaltene and phase behavior of colloids + non-adsorbing polymer + solvent mixtures. Chapter 3 describes the experimental techniques used in this work. The results obtained in the different techniques used are presented, compared and discussed in Chapter 4. Conclusions and recommendations for future work are presented in Chapter 5.

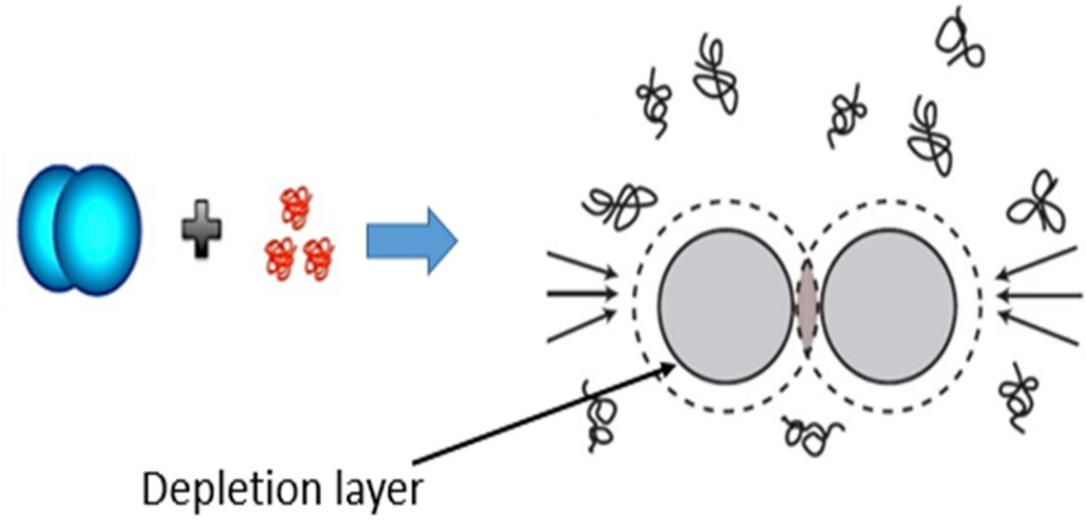

Figure 1.1: A schematic illustration of depletion flocculation mechanism

References

1. Hunter, R. J. (1993). *Introduction to modern colloid science*. Oxford University Press.
2. Dickinson, E., & Eriksson, L. (1991). Particle flocculation by adsorbing polymers. Advances in Colloid and Interface Science, 34, 1-29.
3. Sieglaff, C. L. (1959). Phase separation in mixed polymer solutions. *Journal of Polymer Science Part A: Polymer Chemistry*, *41*(138), 319-326.
4. Murray, B. S., & Phisarnchananan, N. (2014). The effect of nanoparticles on the phase separation of waxy corn starch+ locust bean gum or guar gum. *Food Hydrocolloids*, *42*, 92-99.
5. Tanaka, S., & Ataka, M. (2002). Protein crystallization induced by polyethylene glycol: A model study using apoferritin. *The Journal of chemical physics*, *117*(7), 3504-3510.
6. Poon, W. C. K. (2002). The physics of a model colloid–polymer mixture. Journal of Physics: Condensed Matter, 14(33), R859.
7. Anderson, V. J., & Lekkerkerker, H. N. (2002). Insights into phase transition kinetics from colloid science. Nature, 416(6883), 811.
8. Fleer, G. J., & Tuinier, R. (2008). Analytical phase diagrams for colloids and non-adsorbing polymer. *Advances in colloid and interface science*, *143*(1), 1-47.
9. Khammar, M., & Shaw, J. M. (2012). Estimation of phase composition and size of asphaltene colloidal particles in mixtures of asphaltene+ polystyrene+ toluene at 293 K and atmospheric pressure. Fluid Phase Equilibria, 332, 105-119.
10. Murray, B. S., & Phisarnchananan, N. (2014). The effect of nanoparticles on the phase separation of waxy corn starch+ locust bean gum or guar gum. *Food Hydrocolloids*, *42*, 92-99.

11. AlHammadi, A. A., & Chapman, W. G. (2017). Modeling the Polystyrene–Asphaltenes–Toluene Mixture Using the Perturbed-Chain Form of Statistical Associating Fluid Theory Equation of State. *Energy & Fuels*, *31*(6), 6019-6024.
12. Mullins, O. C., Sheu, E. Y., Hammami, A., & Marshall, A. G. (2007). *Asphaltenes, heavy oils, and petroleomics*. Springer Science & Business Media.
13. Khammar, M., & Shaw, J. M. (2011). Liquid–liquid phase equilibria in asphaltene+ polystyrene+ toluene mixtures at 293 K. *Energy & Fuels*, *26*(2), 1075-1088.
14. Pouralhosseini, S., Alizadehgiashi, M., & Shaw, J. M. (2015). On the Phase Behavior of Athabasca Asphaltene+ Polystyrene+ Toluene Mixtures at 298 K. Energy & Fuels, 29(8), 4855-4863.
15. Amundaraín Hurtado, J. L., Chodakowski, M., Long, B., & Shaw, J. M. (2011). Characterization of physically and chemically separated Athabasca asphaltenes using small-angle X-ray scattering. *Energy & Fuels*, *25*(11), 5100-5112.
16. Zhao, B., & Shaw, J. M. (2007). Composition and size distribution of coherent nanostructures in Athabasca bitumen and Maya crude oil. Energy & Fuels, 21(5), 2795-2804.
17. Maham, Y., Chodakowski, M. G., Zhang, X., & Shaw, J. M. (2005). Asphaltene phase behavior: prediction at a crossroads. Fluid Phase Equilibria, 228, 21-26.

Chapter 2: Literature Review

2.1 Colloidal dispersions

A colloidal dispersion is a macroscopically homogeneous mixture comprising a dispersed particulate phase, whose size is in the 1 nm and 1 μm range for at least one dimension, and a continues liquid medium [1]. Interaction between colloidal particles can be adjusted by adding polymer, electrolytes or by surface modification, changing particle type, solvent, pressure, temperature or by surface modification. Such modification can lead to two-phase or three phase macroscopic behaviours. Complex phase diagrams can arise that can impact the successful operation of existing industrial processes and the design or development of new industrial processes or products, or new remediation strategies wastes arising from industrial processes. Each of these topics is addressed below.

2.2 Interaction among colloidal particles in dispersions

The stability of colloids dispersed in liquid media relies upon the interplay between Brownian and inter particle forces, principally Van der Waals attractive force and electrostatic repulsive force [2]. Figure 2.1 illustrates the net interaction potential vs particle separation distance. Net attractive potentials are negative and tend to destabilize colloidal dispersions. Net repulsive forces represented by a positive potential tend to stabilize them.

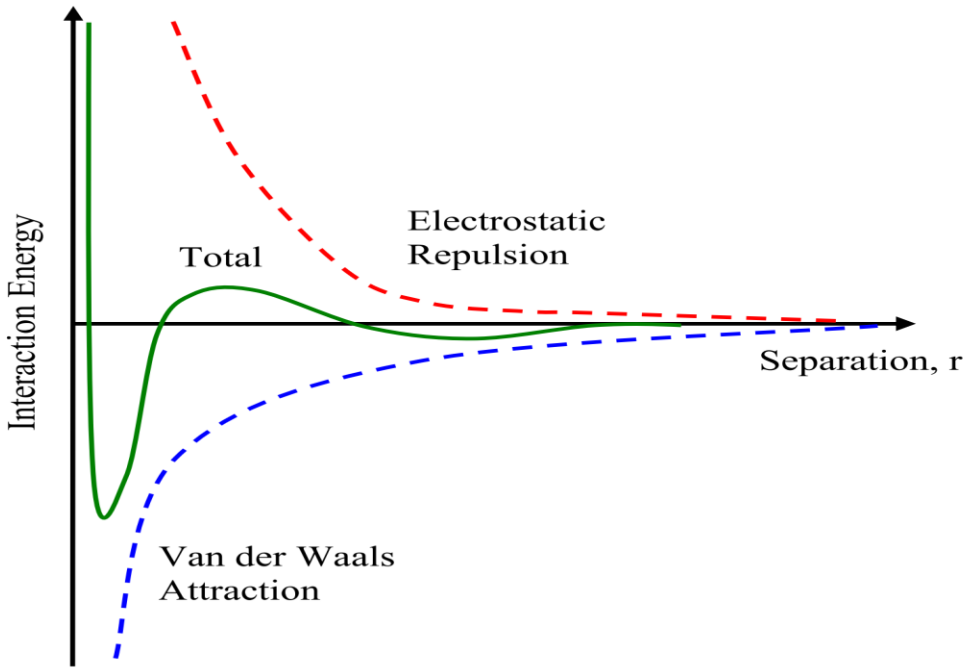

Figure 2.1: Interaction potential as a function of particle separation distance

2.3 Interactions between polymer molecules and colloidal particles

The addition of polymer into colloidal dispersions can induce bridging or depletion flocculation depending on whether polymer molecules adsorbs on particle surfaces or not. The physics and chemistry impacts are complex. For adsorbing polymers, at low to moderate polymer concentration, polymers may adsorb onto two or more particles and form bridges leading to bridging flocculation (Figure 2.2a), while at high polymer concentration, surfaces of the colloidal particles are covered by polymer and this may result in steric stabilization (Figure 2.2b) of the dispersion. Depletion flocculation (Figure 2.2c) only arises if the polymer does not adsorb. The polymer concentration must be large enough so that the osmotic pressure difference is large enough to induce a phase transition into colloid rich and polymer rich phases. At high concentrations of non-adsorbing polymer, the thickness of the depletion zones around particles

becomes thinner, as the osmotic pressure increases. This results in restabilization of the colloidal dispersion - an effect known as depletion stabilization (Figure 2.2d) [3 4]. The physical mechanism of depletion stabilization continues to be debated. Recent investigations [5 6 7 8] reveal that the depletion interaction has a short-range depletion attraction and a long-range depletion repulsion. Above a certain polymer concentration, the repulsion energy barrier becomes higher and causes depletion stabilization. This latter effect is of potential importance because it suggests that at fixed nanoparticle composition there can be two transitions as polymer mass fraction is increased and the solvent mass fraction is decreased. The transitions are from a single bulk phase to two bulk phases and then back to a single phase.

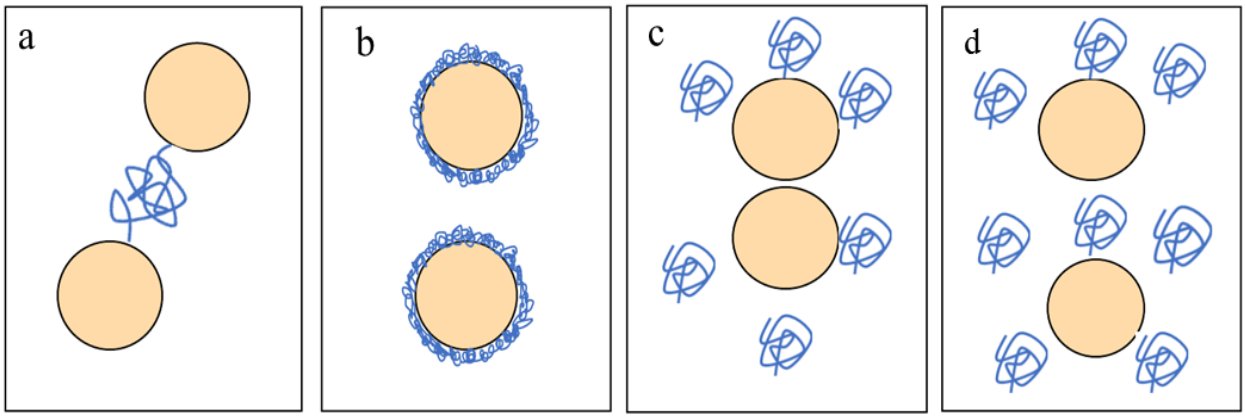

Figure 2.2: Effect of polymer addition on local particle-solvent-polymer interaction in colloidal mixtures: a) Bridging flocculation b) Steric stabilization c) Depletion flocculation d) Depletion stabilization

2.4 Colloidal state of asphaltenes

Asphaltenes a complex component of crude oil can be separated from crude oils by "precipitation" using non-polar solvents like heptane or pentane [9]. In crude oil and solvents such as toluene and benzene, petroleum asphaltenes are wholely or largely nano aggregated [10 11 12]. The size and shape of the asphaltene nano-aggregates in crude oil and toluene continue to be debated in the literature based on experimental observations using a variety of experimental techniques from centrifugation, to filtration and dynamic light scattering, and from rheological, to SANS/SAXS measurements. Number and mass mean properties are not well delineated. Number means tend to be much smaller than mass means. For chemically separated asphaltenes in toluene, the diameter of asphaltene nano particles depends on their concentration and reported values range from less then 1.5nm to 16nm [13 14 15]. Sizes of asphaltene rich nanoaggregated materials in crude oils can be determined by nanofiltration. Data obtained in this way possess broad size distributions with maxima ~ 100 nm and minima less than 5 nm [16 17 18 19].

2.5 Effect of polymer addition on the behaviour of asphaltene + solvent mixtures

Polymers can be used as dispersants to control asphaltene sedimentation. Kabel et al. [20] studied various dendronized polyamidoamine (PAMAM) polymers (Figure 2.3) as potential dispersants and found that a third generation (G3) dendrimer of PAMAM was most successful due to high degree of branching which causes steric hindrance between asphaltene aggregates. Chavez-Miyauchi et al. [22] explored the asphaltene dispersive effect of various polyisobutylene succinimides (Figure 2.4) in heptane. The results showed that succinimides with both benzene structures and hydroxyl groups were most successful. Chang and Fogler [23] investigated several

alkyl-benzyne-derived amphiphiles to stabilize asphaltene in aliphatic solvents. They found that the attraction between

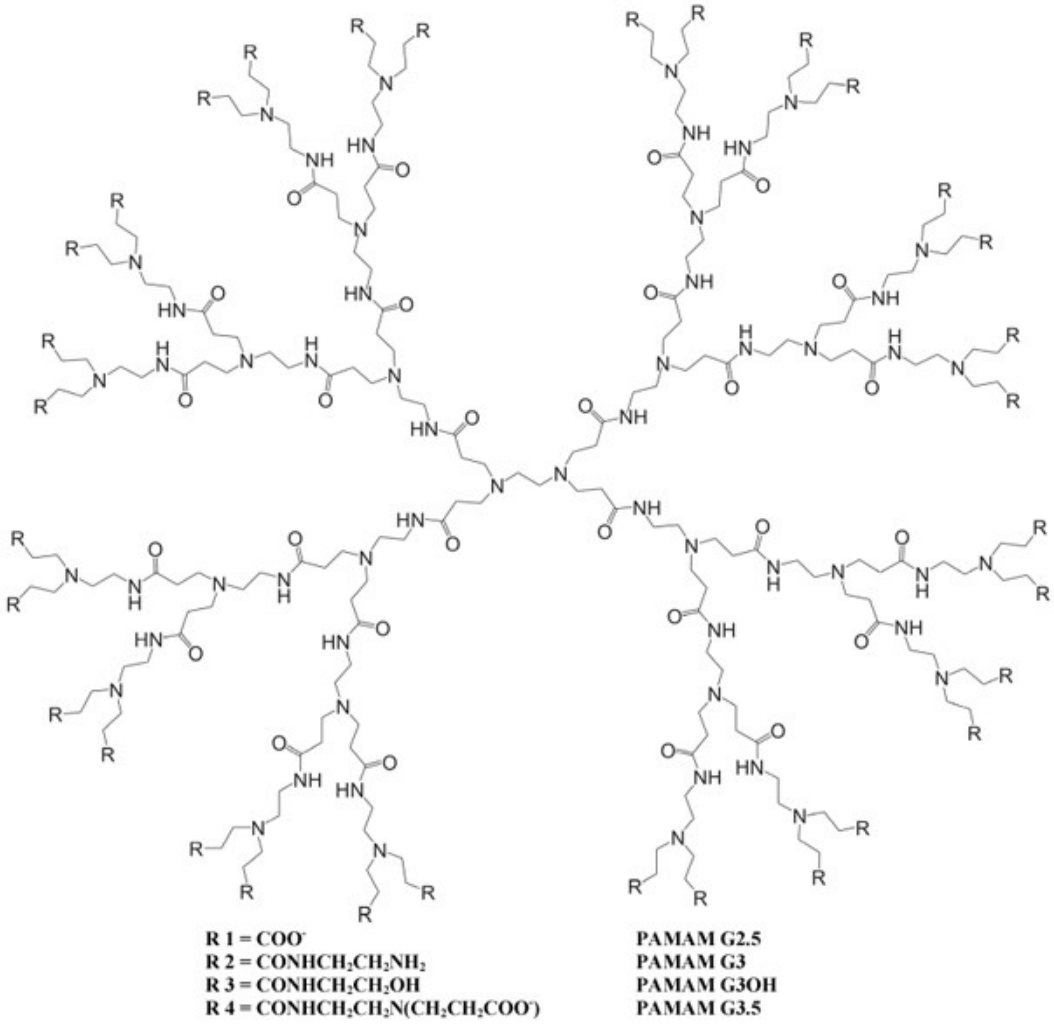

Figure 2.3: Structure of PAMAM dendrimer [21]

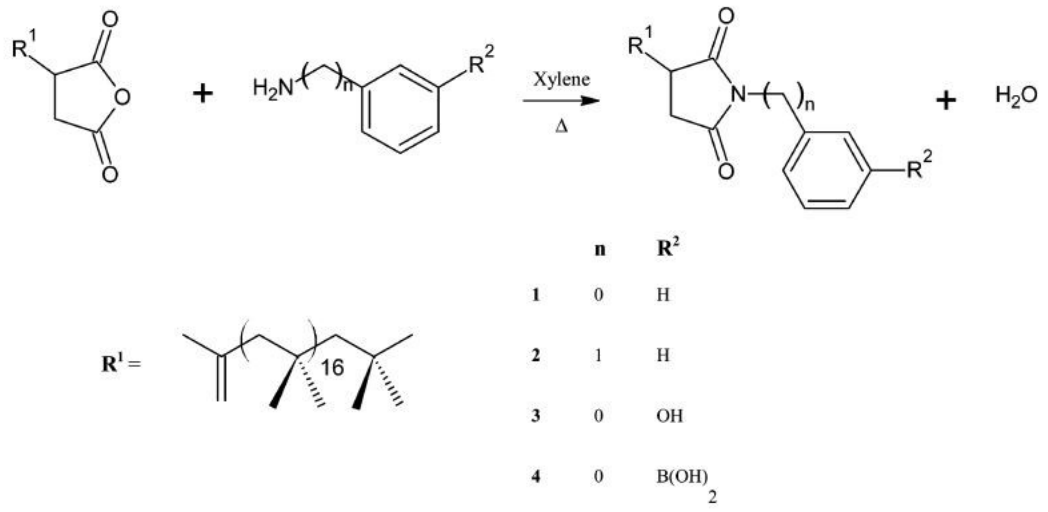

Figure 2.4: synthetic route of aromatic polyisobutenyl succinimides [22]

amphiphiles and asphaltenes can be strengthened by increasing the polarity of the amphiphile head group, and thereby improves asphaltene stabilization. Hashmi et al. [24] studied the effectiveness of polyolefin amide alkeneamine polymeric dispersants and alkylated phenol to render stability of asphaltene in mixtures of oil + heptane. They showed that a delay in asphaltene sedimentation was caused by the reduction in asphaltene particle size and change of interactions among asphaltene particles. According to Lima et al. [25] polymers that contain polar groups are most suitable for altering asphaltene stability. They tested two different sets of polymers, polycardanol with different molar masses and sulfonated polystyrene with various degrees of sulfonation. They showed that both polymers act as flocculants at low concentration and dispersants at higher concentrations. They also stated, but did not demonstrate, that polymers like polystyrene (without polar groups) do not induce phase separation. Khammar et al. [26] showed that polystyrene does induce phase separation via the depletion flocculation mechanism. They also demonstrated that asphaltenes in toluene are wholely or largely nanoparticulate in nature because depletion

flocculation would not otherwise occur. The phase behavior of asphaltene rich nanoaggregates in naturally occurring hydrocarbon + polystyrene + toluene mixtures have yet to be explored.

2.6 Asphaltenes as a representative of the nanoaggregates in oil:

Asphaltenes are surrogates for nanoaggregates present in oil with which they share many but not all properties. Asphaltenes are defined as a fraction of crude oil or bitumen that can be separated from oil using n-alkane (usually n-pentane or n-heptane). Pentane asphaltenes represents the nanoaggregates in oil better than heptane asphaltenes from the perspective of X-ray scattering, elemental analysis and particle density measurement [27]. However, compositions and phase behaviors of chemically separated asphaltenes, on which correlations and models are largely based, are not good representatives of the nanoaggregates in crude oils [28]. There are several aggregation + precipitation models that based on chemically separated asphaltenes and they have a high rate of failure. For example, the De Boor plot [29] is based on chemically separated asphaltene and used widely for evaluating the risk of asphaltene precipitation during depressurization. This plot describes three regions: one where no deposition problems are expected, one where problems may arise and one where severe problems are expected, as shown in the Figure 2.5, where blue dots represent real fields without production problems and red dots represents fields with known production problems. The De Boor approach fails frequently.

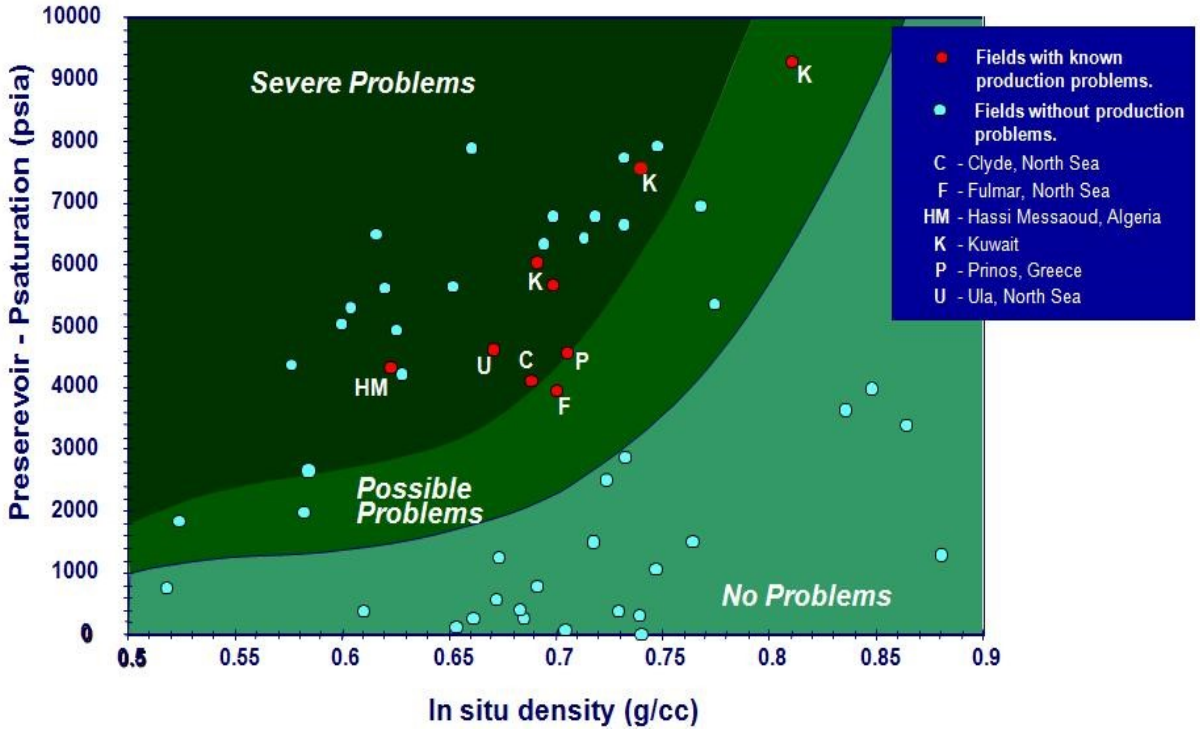

Figure 2.5: De Boer plot with field data [30]

2.7 Phase behavior of non-adsorbing polymer + solvent + nanoparticle mixtures

It is well known from experiments that addition of non-adsorbing polymer can induce phase separation by depletion flocculation mechanism. Phase diagrams of a mixture of Colloid + non-adsorbing polymer in a solvent typically show colloid gas or colloidal poor phase, G (containing mainly polymer + solvent), a colloid liquid or colloidal rich phase, L (containing mainly solvent + colloid) and a colloid phase or largely colloidal rich phase, C. Theoretical description of the phase behavior of such mixtures was first given by Asakura and Osowa [31], where they considered both colloids and non-adsorbing polymer as hard spheres and later developed by others [32 33 34] using thermodynamic perturbation theory. At low colloid and polymer mass fraction, the topology of phase diagrams for such mixtures are sensitive to the ratio R_g/a, where R_g is the polymer radius

of gyration and a is the radius of colloidal particles. For $a>>R_g$, single colloidal gas (G) and colloidal rich (C) phases are observed separated by a two phase CG region [35]. Lekkerkerker et al [36] developed an osmotic equilibrium or free volume theory (FVT), to predict the phase behavior of such mixtures using statistical mechanics. Fleer et al. [37] generalized free volume theory (GFVT). According to this theory, the depletion thickness δ depends on size ratio, R_g/a and polymer volume fraction in the mixture. Fleer et al. [38] compared experimental data with their theory for $\frac{R_g}{a} = 1$. The gas-liquid (GL) binodal and three phase region (G+L+C) are in good agreement with this model, as shown in the Figure 2.6. The agreement between this model and Monte Carlo simulation for mixtures of hard spheres and self-avoiding polymer chains is also quite good [39].

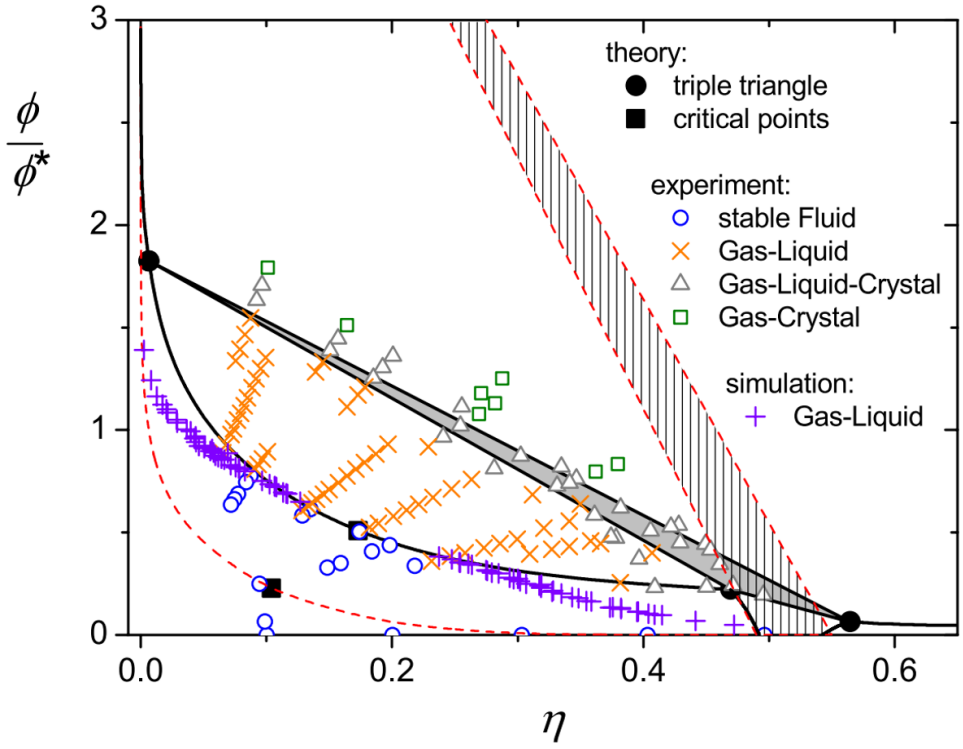

Figure 2.6: Phase diagram of a colloid and non-adsorbing polymer mixture for Rg/a =1 [38]. Crosses, squares and triangles represents experimental GL, GLC and GC regions respectively. (○) stable one phase. Theoretical regions for triple phase existence (GLC) predicted by FVT [36] (----) and GFVT [33] (—). Binodals of FC, GL and GC are depicted as (----) (FVT) and (—) (GFVT) curves. (●) The composition of coexisting GLC phases at the triple point predicted by GFVT. (+) Monte Carlo simulation result.

The Fleer et al. [37] model is a monodispersed model and cannot be used directly for polydispersed colloids with polymers in solvents. Khammar et al [40]. studied pentane asphaltene + polystyrene (non-adsorbing polymer) + toluene mixtures and observed phase separation due to depletion flocculation. In their work, the composition of the phases in mixtures of asphaltene + polystyrene + toluene were determined using the procedure described by Bodnar et al [41]. It is initially assumed that all asphaltene colloidal particles participated in the phase separation mechanism.

Calculated binodal compositions were then used to calculate the speeds of sound in the phases and the values were compared with measured speed of sound values. They introduced a concentration independent fraction γ of asphaltene colloidal particles participating in the phase separation mechanism to match calculated speed of sound with experimental results. Then, Khammar et al. [40] used the Fleer et al. model to compare the experimental results with predicted ones. As both the polystyrene and the asphaltenes are polydispersed, only qualitative agreement was obtained as shown in Figure 2.7. The location of the critical point can be approximated by manipulating the mean particle size of asphaltene particles even though the phase boundary is poorly represented.

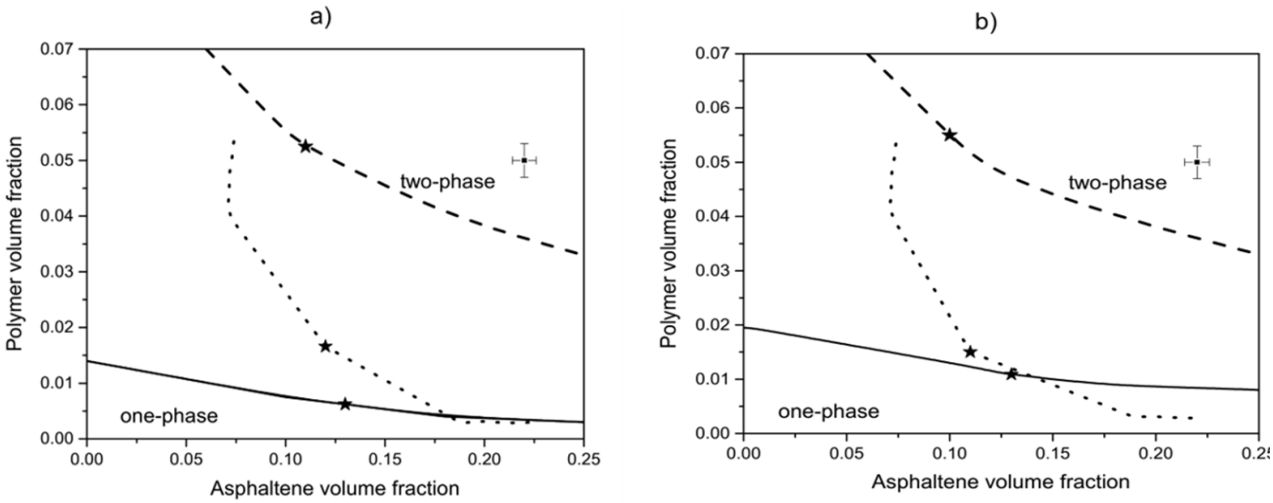

Figure 2.7: Calculated phase diagram using Fleer et al. method vs. experimental phase diagram (**…..**) for mixtures of Maya asphaltene colloidal particles + polystyrene + toluene for polystyrene molar masses: a) 393,000 g/mol and b) 700,000 g/mol and for two radii of asphaltenes nanoparticles, (**----**): a=6.4 nm, (—) curve: a=23.5 nm [40]. (★)critical points.

Sajjad et al. [42] modified the Fleer et al. [37] method by introducing aspahltene mean particle size and the fraction of asphaltene particles participating in the phase separation mechanism as a function of global composition. As shown in the Figure 2.8a, the calculated phase diagram for

Maya pentane asphaltene + polystyrene + toluene is in good agreement with experimental phase diagram adjacent to the L=G critical point. Chapman et al. [43] used the Perturbed Chain form of the SAFT (PC-SAFT) equation of state to model a sub set of data for the same mixtures. Their approach, used to model phase behavior of polymer solutions and crude oils, also provides quantitative agreement with experimental data (Figure 2.8b) near the L=G critical point.

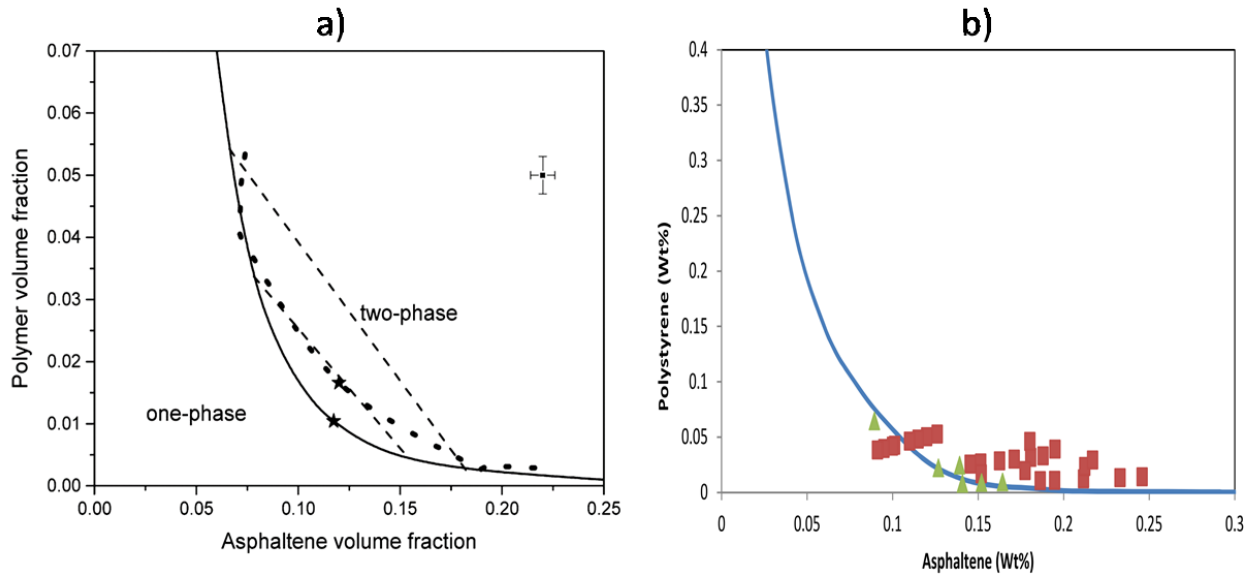

Figure 2.8: a) Calculated phase diagram using the modified Fleer et al. method (—) vs experimental phase diagram (••••) for mixtures of Maya pentane asphaltene colloidal particles + toluene+ polystyrene (393 000 g/mol) at T = 293K and P =1atm. (★): critical point, (---): computed tie lines [42]. b) Phase diagram for mixtures of Maya pentane asphaltene + toluene + polystyrene (400,000 g/mol). (—): PC-SAFT prediction [43], (■): experimental two phase region [26], (▲): experimental one phase region [26].

However, neither model accommodates or accounts for the emergent divergence of the LG/L and LG/G phase boundaries from the asphaltene and polymer axes remote from the critical point seen in the experimental data. Further, neither approach predicts or suggests that depletion restabililization at high polymer concentration may impact the phase behaviour of nanoparticle + solvent + non adsorbing polymer mixtures. For example, Kumar [44] and Kumar and Shaw [45], show closed loop LG regions and other phase diagrams with two critical points based on the phase behaviour of polystyrene + silica + cyclohexane mixtures and conceptual phase diagrams connecting their observations with phase diagrams for other mixtures, as shown in Figure 2.9. Consequently, it is important to perform experiments at high enough mass fractions of polymer and asphaltenes to explore how experimental LG/L and LG/G phase boundaries behave, in general, and with respect to these models for asphaltene containing mixtures in particular.

The possibility of a closed loop two-phase region is tantalizing, particularly as this would imply the presence of a second critical point on the two-phase to one phase boundary that does not appear to be accounted for in the phase behaviour models for nanoparticle + polymer + solvent phase behaviour in general and for asphaltene + polymer + toluene mixtures in particular. Pursuit of this goal is the principal objective of this thesis. Experimental methods, as described in Chapter 3, are pushed to their limits.

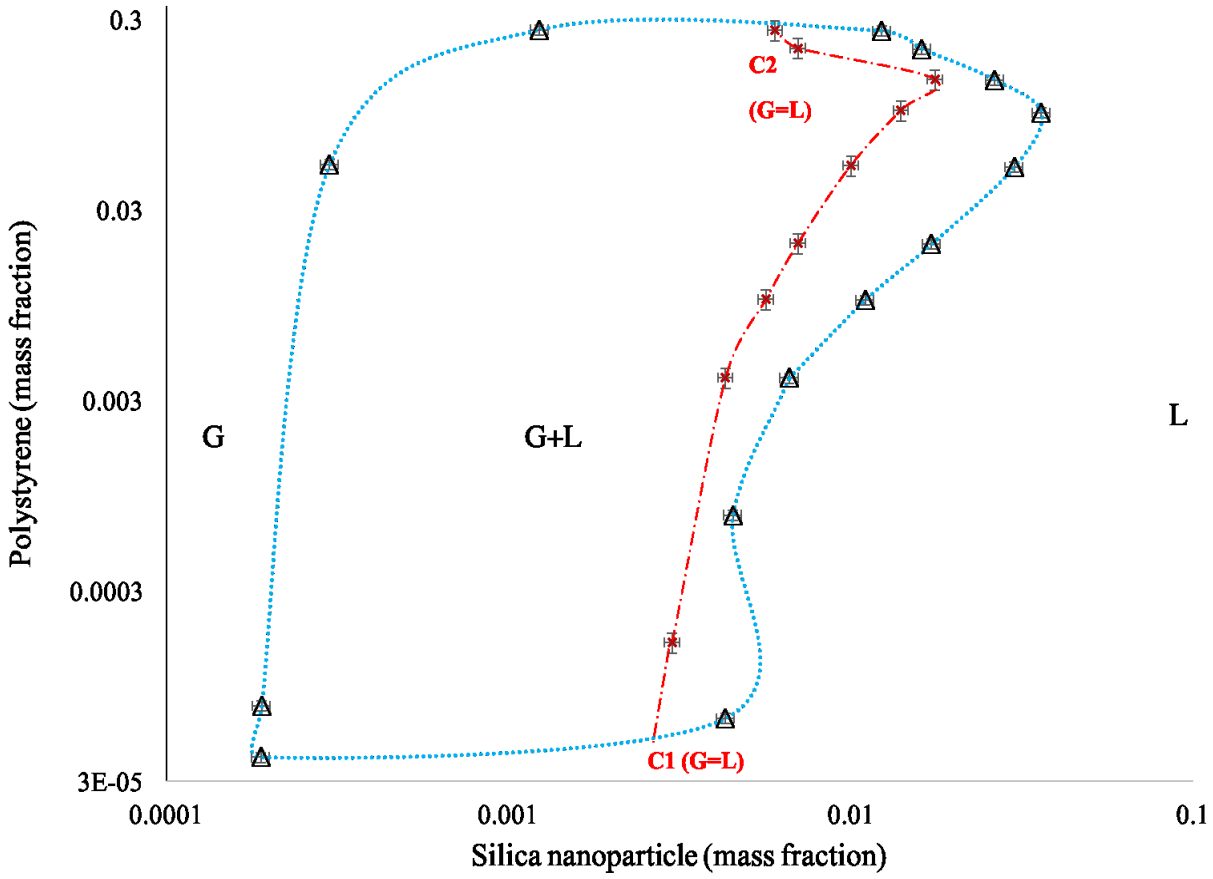

Figure 2.9: Experimental phase diagram of cyclohexane + polystyrene + silica nanoparticles at 303 K. (△) G+L phase boundary, and (x) G=L=0.5 (volume fraction), (C1) first critical point, and (C2) second critical point [44].

References

1. Hiemenz, P. C., & Rajagopalan, R. (Eds.). (1997). *Principles of Colloid and Surface Chemistry, revised and expanded* (Vol. 14). CRC press.
2. Russel, W. B., Saville, D. A., & Schowalter, W. R. (1989). *Colloidal dispersions*. Cambridge university press.
3. Fleer, G. J., & Scheutjens, J. M. H. M. (1987). Effect of adsorbing and nonadsorbing polymer on the interaction between colloidal particles. *Croatica Chemica Acta*, *60*(3), 477-494.
4. Kim, S., Hyun, K., Moon, J. Y., Clasen, C., & Ahn, K. H. (2015). Depletion stabilization in nanoparticle–polymer suspensions: multi-length-scale analysis of microstructure. Langmuir, 31(6), 1892-1900.
5. Walz, J. Y., & Sharma, A. (1994). Effect of long range interactions on the depletion force between colloidal particles. Journal of colloid and interface science, 168(2), 485-496.
6. Mao, Y., Cates, M. E., & Lekkerkerker, H. N. W. (1995). Depletion force in colloidal systems. Physica A: Statistical Mechanics and its Applications, 222(1-4), 10-24.
7. Semenov, A. N. (2008). Theory of colloid stabilization in semidilute polymer solutions. Macromolecules, 41(6), 2243-2249.
8. Crocker, J. C., Matteo, J. A., Dinsmore, A. D., & Yodh, A. G. (1999). Entropic attraction and repulsion in binary colloids probed with a line optical tweezer. Physical review letters, 82(21), 4352
9. Speight, J. G., & Moschopedis, S. E. (1981). On the molecular nature of petroleum asphaltenes.
10. Sheu, E. Y., Storm, D. A., & Maureen, M. (1991). Asphaltenes in polar solvents. *Journal of non-crystalline solids*, *131*, 341-347.

11. Overfield, R. E., Sheu, E. Y., Sinha, S. K., & Liang, K. S. (1989). SANS study of asphaltene aggregation. *Fuel science & technology international*, *7*(5-6), 611-624.
12. Dwiggins, C. W. (1978). Study of colloidal nature of petroleum with an automated Bonse–Hart X-ray small-angle scattering unit. *Journal of Applied Crystallography*, *11*(5), 615-619.
13. Mostowfi, F., Indo, K., Mullins, O. C., & McFarlane, R. (2008). Asphaltene nanoaggregates studied by centrifugation. *Energy & fuels*, *23*(3), 1194-1200.
14. Espinat, D., Fenistein, D., Barre, L., Frot, D., & Briolant, Y. (2004). Effects of temperature and pressure on asphaltenes agglomeration in toluene. A light, X-ray, and neutron scattering investigation. *Energy & fuels*, *18*(5), 1243-1249.
15. Barré, L., Simon, S., & Palermo, T. (2008). Solution properties of asphaltenes. *Langmuir*, *24*(8), 3709-3717.
16. Ching, M. J. T. M., Pomerantz, A. E., Andrews, A. B., Dryden, P., Schroeder, R., Mullins, O. C., & Harrison, C. (2010). On the nanofiltration of asphaltene solutions, crude oils, and emulsions. *Energy & Fuels*, *24*(9), 5028-5037.
17. Zhao, B., & Shaw, J. M. (2007). Composition and size distribution of coherent nanostructures in Athabasca bitumen and Maya crude oil. *Energy & Fuels*, *21*(5), 2795-2804.
18. Sheu, E. Y. (2006). Small angle scattering and asphaltenes. Journal of Physics: Condensed Matter, 18(36), S2485.
19. McKenna, A. M., Blakney, G. T., Xian, F., Glaser, P. B., Rodgers, R. P., & Marshall, A. G. (2010). Heavy petroleum composition. 2. Progression of the Boduszynski model to the limit of distillation by ultrahigh-resolution FT-ICR mass spectrometry. Energy & Fuels, 24(5), 2939-2946.

20. Kabel, K. I., Abdelghaffar, A. M., Farag, R. K., Maysour, N. E., & Zahran, M. A. (2015). Synthesis and evaluation of PAMAM dendrimer and PDPF-b-POP block copolymer as asphaltene inhibitor/dispersant. *Research on Chemical Intermediates*, *41*(1), 457-474.
21. Fernández, L., Sigal, E., Otero, L., Silber, J. J., & Santo, M. (2011). Solubility improvement of an anthelmintic benzimidazole carbamate by association with dendrimers. Brazilian Journal of Chemical Engineering, 28(4), 679-689.
22. Chávez-Miyauchi, T. E., Zamudio-Rivera, L. S., & Barba-López, V. (2013). Aromatic polyisobutylene succinimides as viscosity reducers with asphaltene dispersion capability for heavy and extra-heavy crude oils. *Energy & Fuels*, *27*(4), 1994-2001.
23. Chang, C. L., & Fogler, H. S. (1994). Stabilization of asphaltenes in aliphatic solvents using alkylbenzene-derived amphiphiles. 1. Effect of the chemical structure of amphiphiles on asphaltene stabilization. *Langmuir*, *10*(6), 1749-1757.
24. Hashmi, S. M., Quintiliano, L. A., & Firoozabadi, A. (2010). Polymeric dispersants delay sedimentation in colloidal asphaltene suspensions. *Langmuir*, *26*(11), 8021-8029.
25. Lima, A. F., Mansur, C. R., Lucas, E. F., & González, G. (2010). Polycardanol or sulfonated polystyrene as flocculants for asphaltene dispersions. *Energy & Fuels*, *24*(4), 2369-2375.
26. Khammar, M., & Shaw, J. M. (2011). Liquid–liquid phase equilibria in asphaltene+ polystyrene+ toluene mixtures at 293 K. *Energy & fuels*, *26*(2), 1075-1088.
27. Eyssautier, J., Espinat, D., Gummel, J., Levitz, P., Becerra, M., Shaw, J., & Barré, L. (2011). Mesoscale organization in a physically separated vacuum residue: comparison to asphaltenes in a simple solvent. Energy & Fuels, 26(5), 2680-2687.

28. Amundaraín Hurtado, J. L., Chodakowski, M., Long, B., & Shaw, J. M. (2011). Characterization of physically and chemically separated Athabasca asphaltenes using small-angle X-ray scattering. *Energy & Fuels*, *25*(11), 5100-5112.
29. De Boer, R. B., Leerlooyer, K., Eigner, M. R. P., & Van Bergen, A. R. D. (1995). Screening of crude oils for asphalt precipitation: theory, practice, and the selection of inhibitors. SPE Production & Facilities, 10(01), 55-61.
30. Oilfieldwiki.com. (2018). File:Deboer.jpg - OilfieldWiki. [online] Available at: http://www.oilfieldwiki.com/wiki/File:Deboer.jpg [Accessed 3 May 2018].
31. Asakura, S., & Oosawa, F. (1954). On interaction between two bodies immersed in a solution of macromolecules. *The Journal of Chemical Physics*, *22*(7), 1255-1256.
32. Gast, A. P., Hall, C. K., & Russel, W. B. (1983). Polymer-induced phase separations in nonaqueous colloidal suspensions. *Journal of Colloid and Interface Science*, *96*(1), 251-267.
33. Gast, A. P., Russel, W. B., & Hall, C. K. (1986). An experimental and theoretical study of phase transitions in the polystyrene latex and hydroxyethylcellulose system. *Journal of colloid and interface science*, *109*(1), 161-171.
34. Vincent, B., Edwards, J., Emmett, S., & Croot, R. (1988). Phase separation in dispersions of weakly-interacting particles in solutions of non-adsorbing polymer. *Colloids and Surfaces*, *31*, 267-298.
35. Jenkins, P., & Snowden, M. (1996). Depletion flocculation in colloidal dispersions. *Advances in colloid and interface science*, *68*, 57-96.
36. Lekkerkerker, H. N. W., Poon, W. K., Pusey, P. N., Stroobants, A., & Warren, P. 0. (1992). Phase behaviour of colloid+ polymer mixtures. *EPL (Europhysics Letters)*, *20*(6), 559.

37. Fleer, G. J., & Tuinier, R. (2008). Analytical phase diagrams for colloids and non-adsorbing polymer. *Advances in colloid and interface science*, *143*(1-2), 1-47.

38. Tuinier, R., Smith, P. A., Poon, W. C. K., Egelhaaf, S. U., Aarts, D. G. A. L., Lekkerkerker, H. N. W., & Fleer, G. J. (2008). Phase diagram for a mixture of colloids and polymers with equal size. *EPL (Europhysics Letters)*, *82*(6), 68002.

39. Antl, L., Goodwin, J. W., Hill, R. D., Ottewill, R. H., Owens, S. M., Papworth, S., & Waters, J. A. (1986). The preparation of poly (methyl methacrylate) latices in non-aqueous media. *Colloids and Surfaces, 17*(1), 67-78.

40. Khammar, M., & Shaw, J. M. (2012). Estimation of phase composition and size of asphaltene colloidal particles in mixtures of asphaltene+ polystyrene+ toluene at 293 K and atmospheric pressure. *Fluid Phase Equilibria*, *332*, 105-119.

41. Bodnár, I., & Oosterbaan, W. D. (1997). Indirect determination of the composition of the coexisting phases in a demixed colloid polymer mixture. *The Journal of chemical physics*, *106*(18), 7777-7780.

42. Pouralhosseini, S., Eslami, F., Elliott, J. A., & Shaw, J. M. (2016). Modeling the Phase Behavior of Asphaltene+ Toluene+ Polystyrene Mixtures A Depletion Flocculation Approach. *Energy & Fuels*, *30*(2), 904-914.

43. AlHammadi, A. A., & Chapman, W. G. (2017). Modeling the Polystyrene–Asphaltenes–Toluene Mixture Using the Perturbed-Chain Form of Statistical Associating Fluid Theory Equation of State. *Energy & Fuels*, *31*(6), 6019-6024.

44. Kumar, A. (2018). The Interaction between Depletion Flocculation and Molecular Liquid-Liquid Phase Separation Mechanisms. (MSc thesis, University of Alberta)

45. Kumar, A. & Shaw, J. M. (2018). Combining Depletion Re-stabilization and Depletion Flocculation Effects in Phase Diagrams for Colloid + Polymer Mixtures (in preparation).

Chapter 3: Experimental

3.1 Materials

Toluene 99% was purchased from Fisher Scientific. Polystyrene with average molecular weights Mw= 400,000 g/mol and density = 1.05g/mL was purchased from Aldrich. Asphaltene rich retentate fractions of Athabasca bitumen, were separated from crude oil by Nanofiltration. Pentane asphaltenes were prepared from Athabasca bitumen (AB) according to ASTM D4055. Nanofiltered samples of Athabasca Bitumen, retentate and permeate, were characterized using American Society for Testing and Materials (ASTM) methods. ASTM D5291 was used for carbon, hydrogen, and nitrogen content. ASTM D1552 was used for total sulfur content. These measurements were performed by the Chemistry Department at the University of Alberta. ASTM D2007 was used for SARA fractions and these measurements were performed at the NRC laboratory Devon. The results are summarized in Table 3.1. The measured density of retentate and asphaltenes were 1.06 g/mL and 1.18 g/mL respectively at 298K.

Table 3.1: Composition of Nano-Filtered samples of Athabasca Bitumen (AB)

	AB permeate	AB retentate
	Elemental analysis wt %	
C	83.89	81.58
H	10.63	9.31
N	0.41	0.75
S	4.48	6.43
	SARA analysis wt%	
Saturates	21.15	9.40
Aromatics	48.68	25.74
Resins	27.96	21.76
Asphaltene (C5)	2.21	43.10

3.2 Sample Preparation:

A Zirconium membrane with an average pore size of 10nm was used for nanofiltration. A schematic of the nanofiltration apparatus is shown in Figure 3.1. At the beginning of an experiment, 200mL of Athabasca Bitumen was poured into the reservoir. Before filtration, the reservoir was purged with nitrogen several times. All the experiments were performed at 473k and pressure drop across the membrane was not allowed to exceed 7 bar. Filtration was stopped after

4 weeks. Permeate, retentate, and heated feed stock were collected from the shell side of the membrane, inside the membrane tube and from the reservoir respectively. Mixtures of asphaltenes + polystyrene + toluene and retentate + polystyrene + toluene were prepared using a vortex mixer until they appeared homogeneous. They were then sonicated for 5 hours for polymer concentration lower than 10 volume % and 14 hours for polymer concentration higher than 10 volume % at room temperature. All of these mixtures had a similar appearance and were opaque to visible light – Figure 3.2.

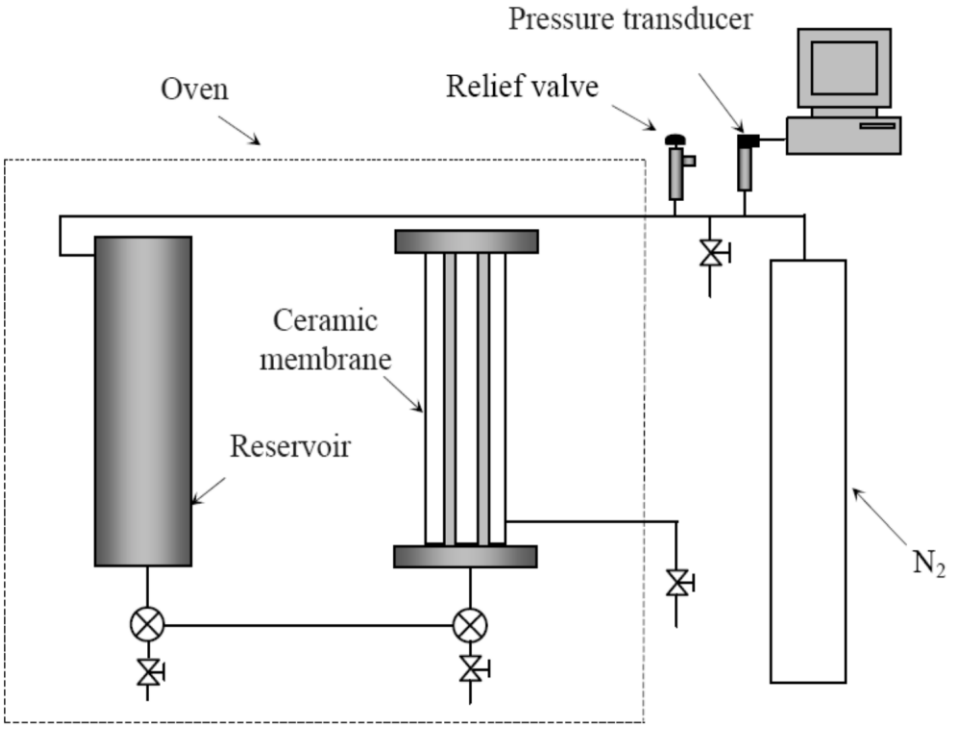

Figure 3.1: Nanofiltration apparatus [1]

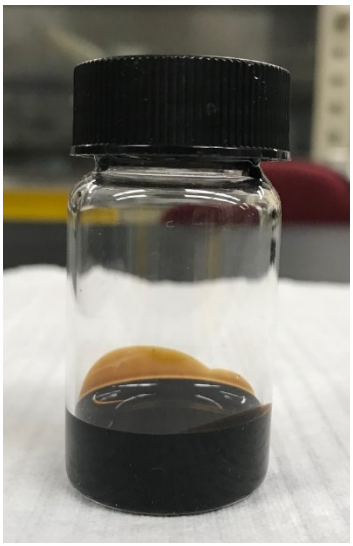

Figure 3.2: A glass vial containing opaque mixture of asphaltene + polystyrene + toluene.

3.3 Measurement of liquid-liquid phase equilibrium

3.4.1 Acoustic View Cell Apparatus

The acoustic view cell apparatus, Figure 3.3, is used to measure times of flight of sound waves through specific path lengths in liquids and solids. Speeds of sound in media are determined based on calibrations with known substances. A detailed description of this equipment can be found elsewhere [2]. A polybenzimidazole cell is used to hold liquid continuous samples during measurements within an aluminum frame. The cell is sealed with a stainless still cap. The temperature inside the cell is controlled with tolerance of ±0.1 K by circulating a mixture of water + ethylene glycol through two copper blocks attached to the cell lid. The acoustic arrays comprising 64 piezoelectric elements over a 35 mm elevation difference are attached to the external walls of the cell by an acoustic coupling gel.

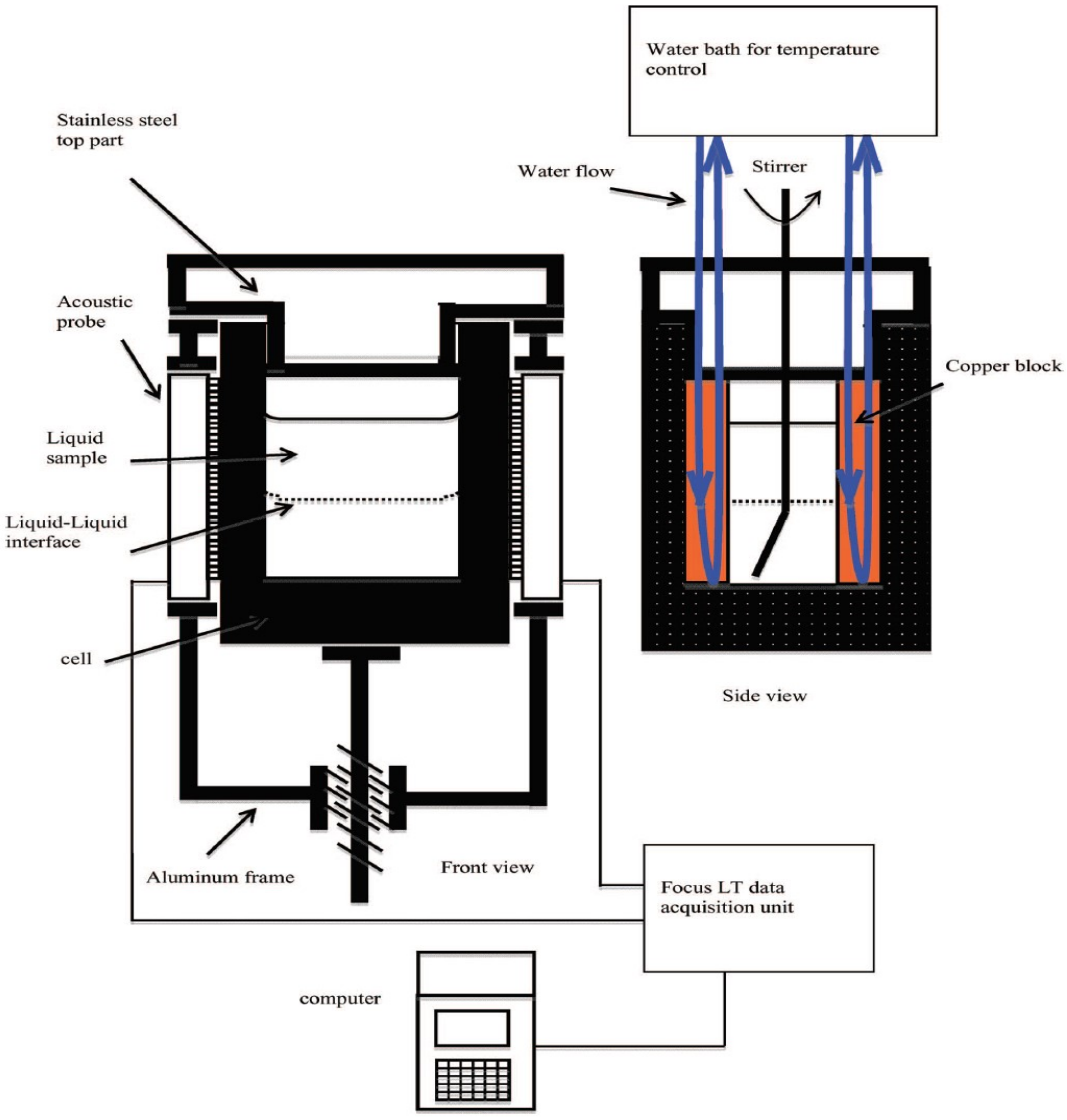

Figure 3.3: Schematic of the acoustic cell

3.4.1.1 Measurement procedure

The acoustic probes are used in sender/receiver mode. The signals are analysed using data acquisition hardware TomoScan Focus LT™ and TomoView™ Software, both from Olympus NDT. Liquid-liquid and liquid-vapor interfaces are identified from the difference in speed of sound with elevation data as illustrated in Figure 3.4. Speed of sound differences as small as 3 m/s across

interfaces are interpretable [2]. Fig 3.5 shows the relation between cell volume and elevation. Precise phase volumes in the two phase region are needed because a method described by Bodnar et al. [3] was used to identify two phase to one phase boundaries. The Bodnar et al. [3] method comprises preparation of mixtures of retentate + toluene + polystyrene that are then diluted by adding aliquots of toluene which are then stirred for 30 minutes. The speed of sound measurements were performed just after removing the stirrer. If no phase separation was observed after 2 hours, mixtures were considered to be single phase. If phase separation was detected then the speed of sound measurements were carried out until there was no change in the volume fraction of two phases. The variation of phase volume fractions along these dilution lines were used to calculate binodal points and critical points. This method was supplemented by direct measurements at compositions in single phase and two-phase regions adjacent to phase boundaries identified to confirm their location.

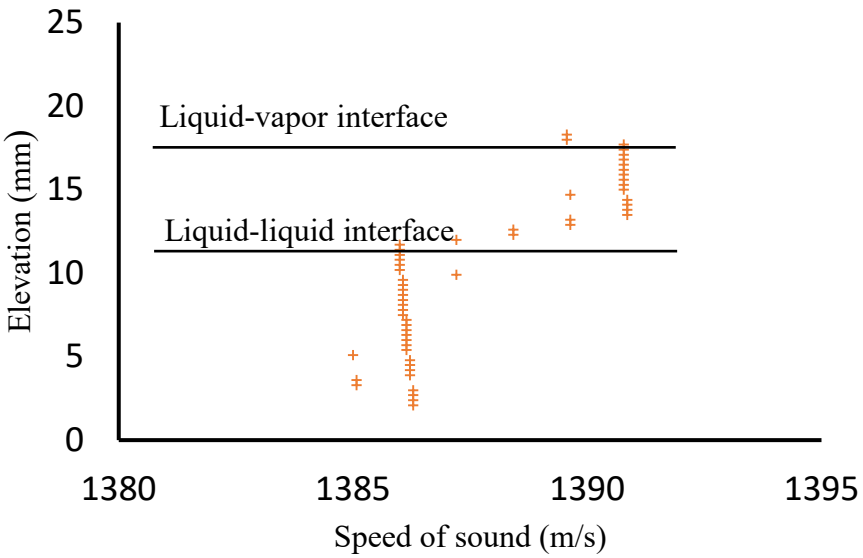

Figure 3.4: Liquid–liquid and liquid–vapor interface detection for AB retentate (15.2 vol%) + toluene (80.6 vol%) + 400,000 g/mol polystyrene (4.2 vol%) at T=298 K.

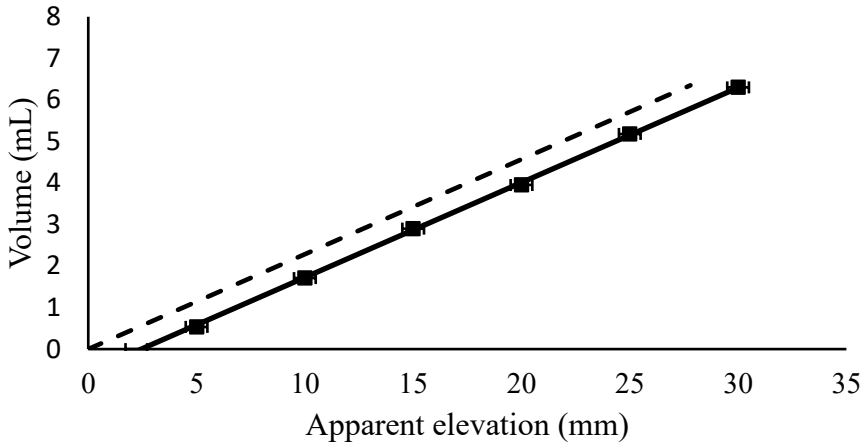

Figure 3.5: Liquid volume vs elevation calibration. (—): apparent elevation measured acoustically; (**----**): elevation from the bottom of cell.

3.4.2 X-ray View Cell Apparatus

A schematic of the X-ray view cell is shown in Figure 3.6. The X-ray view cell apparatus includes an X-ray source (Phillips MCN-165 x-ray generating system) and a camera. A detailed description of this equipment is illustrated elsewhere [4]. A standard glass vial of 22mL containing sample mixtures was placed between the camera and x-ray source. The camera captures the transmitted x-ray beam and these images are monitored and recorded by a computer. The images produced are binary images of 998 by 668 pixels with 256 potential shades of gray. The intensity of the transmitted beam depends on the composition and density of the phases present in the vial. In this work, samples were placed as shown in well calibrated vials and the equipment was operated at room temperature and atmospheric pressure.

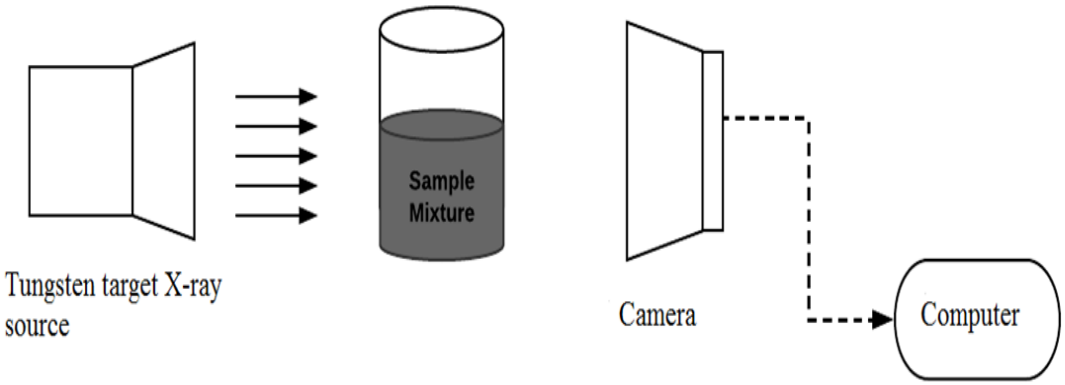

Figure 3.6: X-ray view cell apparatus schematic

3.4.2.1 X-ray tomography physics

X-Ray transmission tomography was used to measure the phase behavior of asphaltene+toluene+polystyrene and retentate+toluene+polystyrene mixtures. Figure 3.7 depicts the fundamentals of the method.

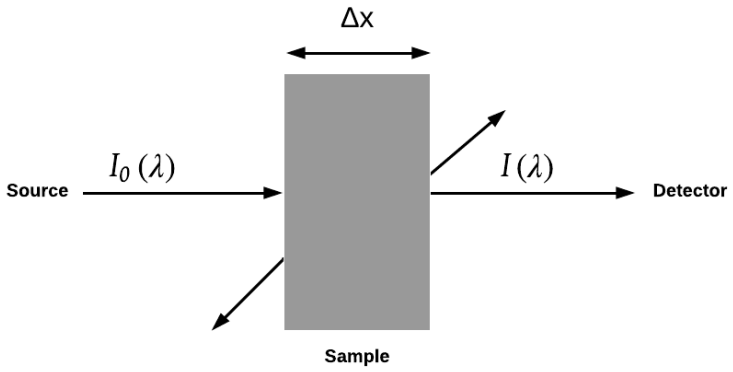

Figure 3.7: Schematic of X-ray absorption

When X-rays emitted from the source, are transmitted through a sample of thickness Δx and density ρ, the intensity of the transmitted beam is expressed as:

$$I(\lambda)= I_0(\lambda) \exp (-\mu(\lambda)\Delta x\rho) \quad (1)$$

Where I_0 is the initial X-ray intensity of the beam and μ is the apparent mass attenuation coefficient of the medium at wavelength λ. For solution or mixtures, the mass attenuation coefficient is obtained by summing the element contributions:

$$\mu = \Sigma_i w_i \mu_i \quad (2)$$

where w_i is the weight fraction of the atomic constituents of a compound.

The absorption of x-ray relies on the kind and quantity of the element as they are absorbed by the core electrons of elements.

3.4.2.2 Quantitative X-ray image analysis

The intensity of the transmitted X-ray beam depends on the composition and density of phases present. Each image of the mixture inside the vial is an average of 300 individual video stills obtained over a period of approximately 3 minutes. A Matlab code was used to analyze these X-ray images. Figure 3.8 shows an example X-ray image with three phases present. Liquid-liquid and liquid-vapor interfaces are clearly visible. Central slices of such images are analyzed quantitatively and elevation differences from the base of the vial to the liquid-liquid and liquid-vapour interfaces are identified +/- 2 pixels as illustrated in Figure 3.9. The relationship between pixel number and phase volume in the 22 mL glass vials, determined by careful calibration with toluene is nearly linear as shown in Figure 3.10. Phase diagrams were constructed systematically from phase volumes and phase volume fractions were obtained from dozens of such images.

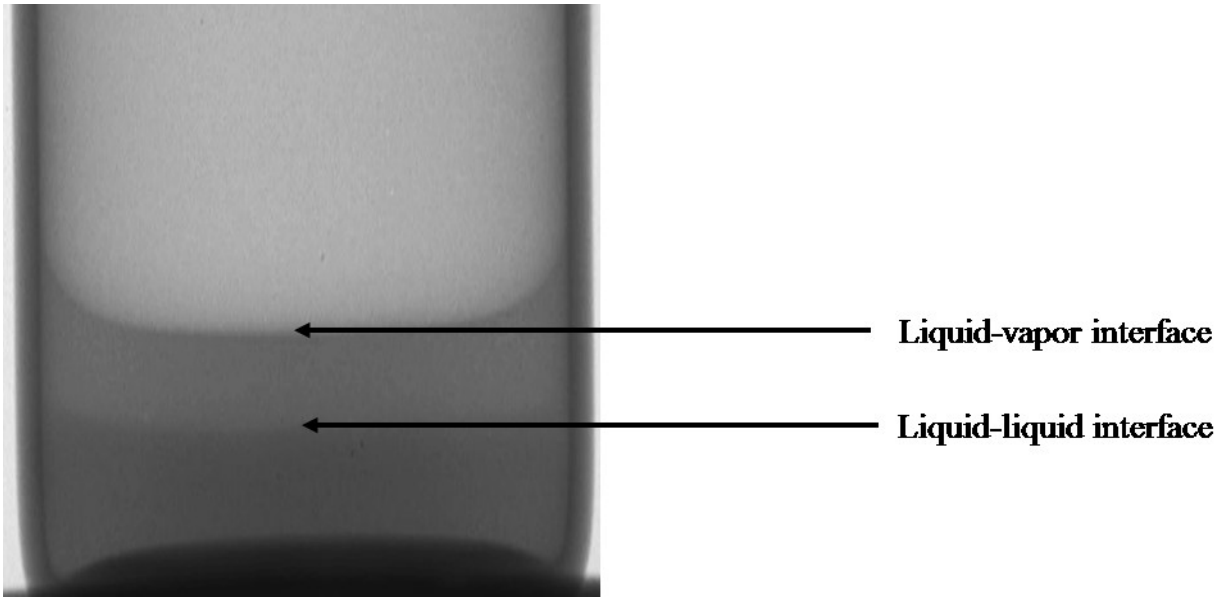

Figure 3.8: X-ray image of asphaltene + polystyrene + toluene

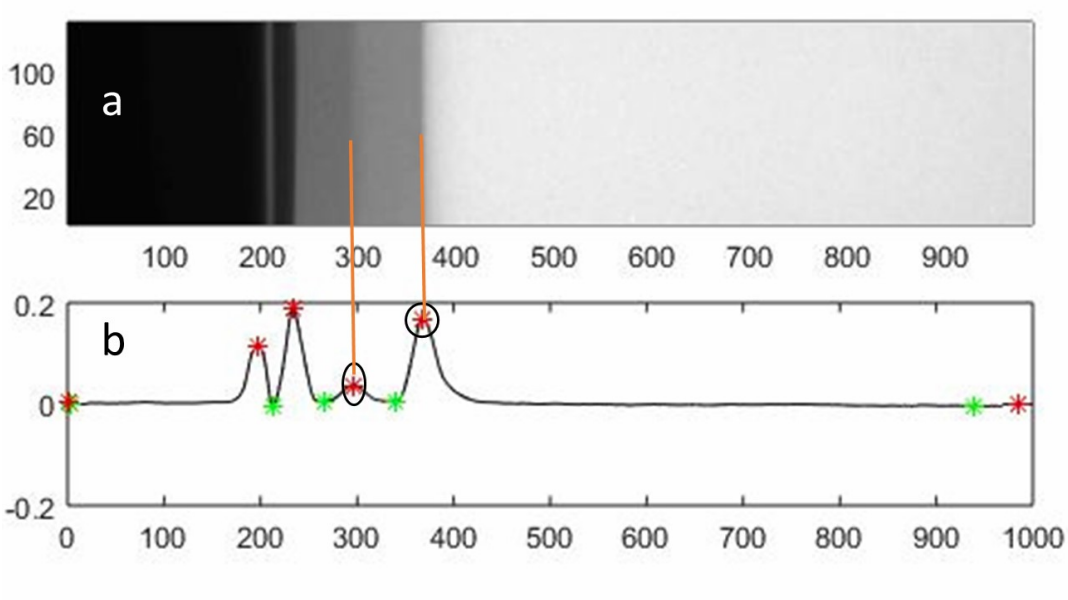

Figure 3.9: Quantitative image analysis of the phase behavior of the asphaltene + polystyrene + toluene mixture shown in Figure 3.8: a) composite image, b) X-ray intensity vs elevation (pixel). The circles with the red asterisks indicate liquid-liquid and liquid-vapor interfaces.

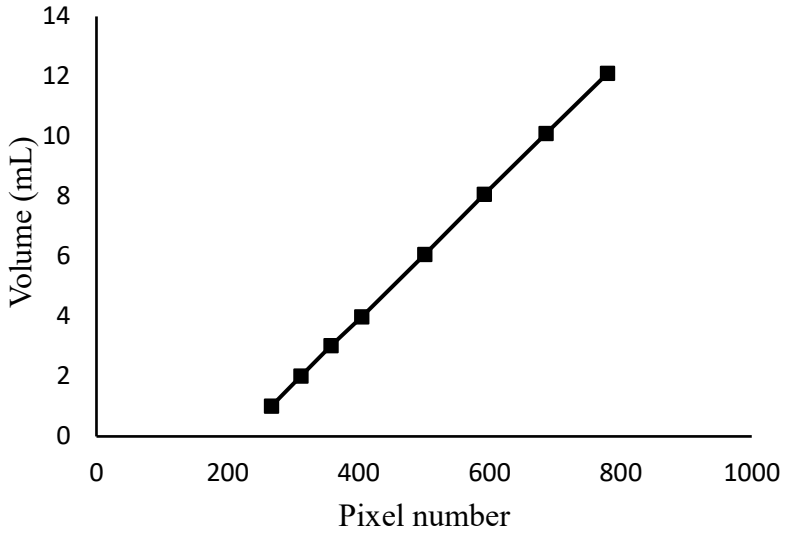

Figure 3.10: Liquid volume vs pixel number for 22 ml vials in the x-ray apparatus.

References:

1. Zhao, B., & Shaw, J. M. (2007). Composition and size distribution of coherent nanostructures in Athabasca bitumen and Maya crude oil. Energy & Fuels, 21(5), 2795-2804.
2. Khammar, M., & Shaw, J. M. (2011). Phase behaviour and phase separation kinetics measurement using acoustic arrays. *Review of Scientific Instruments*, *82*(10), 104902.
3. Bodnár, I., & Oosterbaan, W. D. (1997). Indirect determination of the composition of the coexisting phases in a demixed colloid polymer mixture. *The Journal of chemical physics*, *106*(18), 7777-7780.
4. Abedi, S. J., Cai, H. Y., Seyfaie, S., & Shaw, J. M. (1999). Simultaneous phase behaviour, elemental composition and density measurement using X-ray imaging. *Fluid Phase Equilibria*, *158*, 775-781.

Chapter 4: Results and Discussion

4.1 Phase diagram construction based on acoustic measurements

Phase diagrams for Athabasca pentane asphaltene + polymer + solvent mixtures were prepared previously using acoustic measurements [1]. As one of the principle objectives in this work is to compare phase diagrams for asphaltene rich retentate + polymer + solvent with these data, the same experimental and data processing technique were initially applied. The phase behavior for mixtures of asphaltene rich retentate fraction of heavy oil + polystyrene + toluene were made along dilution line p, q, r as reported in Table A.1 and illustrated in Figure 4.1 using the coordinates polystyrene volume fraction and asphaltene volume fraction. Mixtures were prepared on a mass basis and were converted to volume fractions using densities for asphaltenes, asphaltene rich dispersed material in the retentate, asphaltene free retentate, toluene, and polystyrene of molecular weight 400,000 g/mol respectively. Density values for retentate and pentane asphaltenes and polystyrene obtained by direct measurement were 1.06 g/mL, 1.18 and g/mL, and 1.05 g/mL respectively. Permeate density, also measured, is 0.98 g/mL.

To a first approximation, the density of asphaltene rich material in the retentate can be obtained from:

$$\frac{1}{\rho_r} = \frac{m_o}{\rho_o} + \frac{m_{ar}}{\rho_{ar}} \qquad (1)$$

where,

ρ_r = density of retentate

ρ_o = density of asphaltene free retentate

ρ_{ar} = density of asphaltene in the retentate

m_o = mass fraction of asphaltene free retentate

m_{ar} = mass fraction of asphaltene in the retentate

The density of the permeate is used to approximate the density of the asphaltene free retentate fraction in the retentate. The volume fraction of asphaltene in the retentate is then calculated as:

$$\mathrm{V_{ar}} = (\frac{m_{ar}}{\rho_{ar}})/(\frac{m_o}{\rho_o} + \frac{m_{ar}}{\rho_{ar}}) \quad (2)$$

where,

$\mathrm{V_{ar}}$ = volume fraction of asphaltene in the retentate

and the volume fraction of asphaltene in mixtures of retentate + toluene + polystyrene, V_{aR}, becomes:

$$V_{aR} = \frac{\mathrm{V_{ar}} * volume\ of\ retentate}{volume\ of\ retentate + volume\ of\ toluene + volume\ of\ polystyrene} \quad (3)$$

These dilution lines were created by adding toluene to three different starting mixtures of retentate + polystyrene + toluene. All three starting mixtures separated into two phases where the upper phase is polymer rich, G, and bottom phase is colloid rich, L. After adding sufficient toluene all three dilution lines crossed into a single phase region as shown by the triangle markers in Figure 4.1a. The upper phase volume fraction, R, changes upon addition of toluene as illustrated in Figure 4.1b. Dilution lines p and q trend to R= 1 while dilution line r trends to R=0. At a critical point, the volume fraction of each phase is 0.5 and the composition of each phase becomes identical. The critical point, in this case, is located between dilution lines q and r on the phase boundary. Figure 4.1c shows the two phase to one phase boundary obtained using the method described by Bodnar et al. [2] on the basis of compositions and associated volume fractions along the dilution lines. The boundary was confirmed by additional acoustic measurements. The trajectory for compositions

with equal volume fractions of both phases within the two phase region are also included for reference.

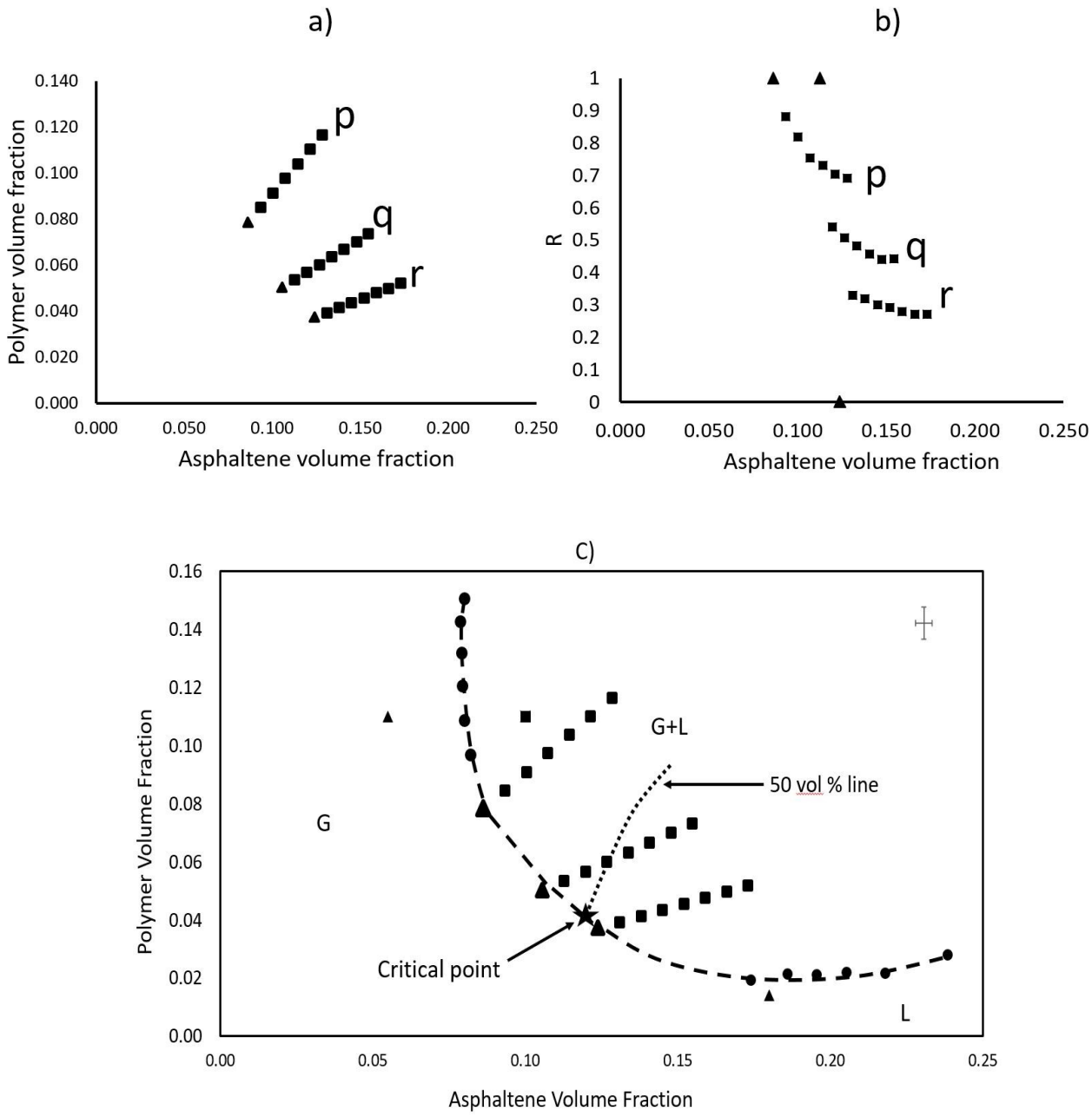

Figure 4.1: Phase behaviour observations of retentate + polystyrene + toluene at 298K identified using speed of sound measurements (a) along dilution lines p, q and r for mixtures; (b) the volume fraction of the upper phase; (c) two phase to one phase boundary construction details. (■): Two-

phase region, (▲): single phase region, (…...): 50 vol% line; (●): computed binodal points from Bodnar's method; (★): critical point. Experimental data are reported in Table A.1 and computed points are reported in Table A.2

4.2 Comparison between asphaltene + polystyrene + toluene and retentate + polystyrene + toluene phase diagrams based on acoustic measurements

The phase diagram for retentate + polystyrene + toluene is compared with the corresponding phase diagram for chemically separated pentane asphaltene + polystyrene + toluene mixtures [1] at 298 K in Figure 4.2. The topology of these phase diagrams is similar. From the relative placement of critical points the average size of the nano-scale particles in the retentate + polystyrene + toluene mixtures is smaller than in asphaltene + polystyrene + toluene mixtures [3].

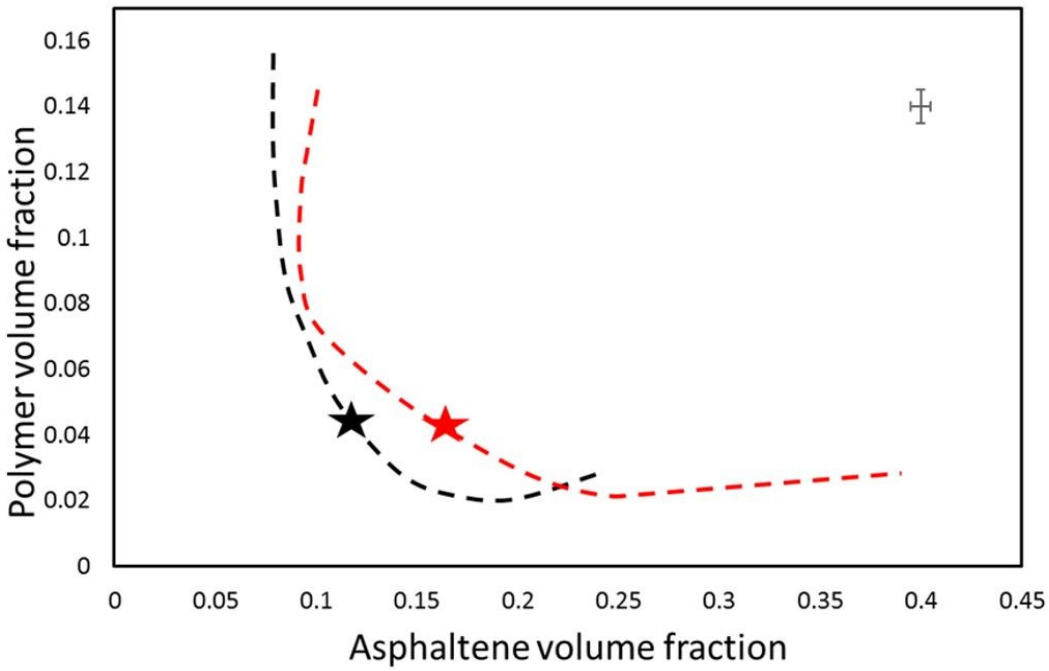

Figure 4.2: Two-phase to one-phase boundary for Athabasca pentane asphaltene + polystyrene + toluene (----) [1] and Athabasca Bitumen retentate + polystyrene + toluene (----) mixtures. (★) Critical point for retentate; (★) critical point for pentane asphaltene.

4.3 Limited sensitivity of acoustic transmission for phase diagram preparation

X-rays images are sensitive to density and composition differences. The X-Ray view cell apparatus, used previously to detect the phase behavior of opaque bitumen + solvent mixtures [4], was used in this work to test and validate the acoustic measurements. Phase diagrams were created using the same construction method, but based on x-ray measurements for pentane asphaltene + polystyrene + toluene mixtures (Figure 4.3 a-c) and retentate + polystyrene + toluene mixtures (Figure 4.4 a-c). Dilution lines p, q, r were created by diluting the mixtures with toluene (Figure 4.3a and Figure 4.4a). The associated volume fractions of upper phase are shown in (Figure 4.3b and 4.4b). The resulting phase diagrams are presented in Figures 4.3c and 4.4c along with

supporting measurements confirming two phase to one phase boundaries. The x-ray and acoustic emission detected phase boundaries are compared in Figure 4.5. For both Athabasca pentane asphaltenes (Figure 4.5a) and retentate (Figure 4.5b) + polystyrene + toluene, the acoustic measurements are too insensitive to detect phase behaviour correctly, particularly in the critical region where differences in phase properties are small. Consequently, acoustic measurements do not provide accurate placement of the critical point and the phase boundaries more broadly and should not be used for these types of mixtures. Previously published data for asphaltene rich mixtures, based acoustic measurements, are invalidated and require correction.

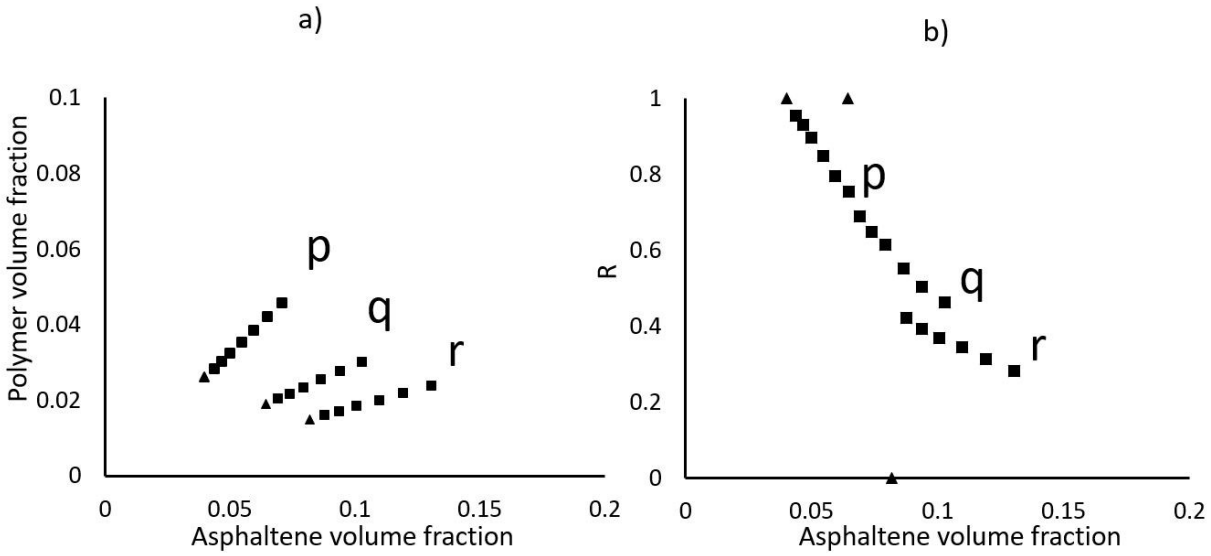

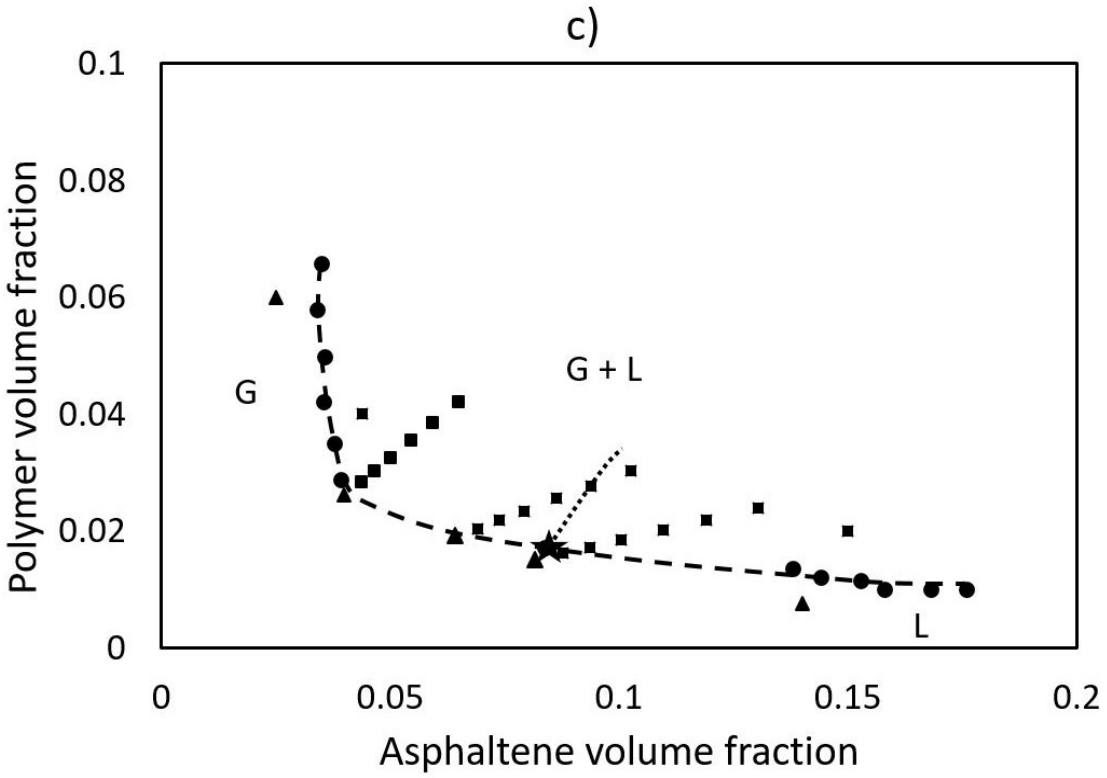

Figure 4.3: Phase behaviour observations (a) along dilution lines p, q and r for mixtures of pentane asphaltene + polystyrene + toluene identified using X-Ray measurements, (b) the volume fraction of the upper phase c) and phase boundary construction details; (■): two-phase; (▲): one-phase; dotted curve: 50 vol% line; (●): binodal points; (★): critical point. Experimental data are reported in Table A.3 and computed points are reported in Table A.4

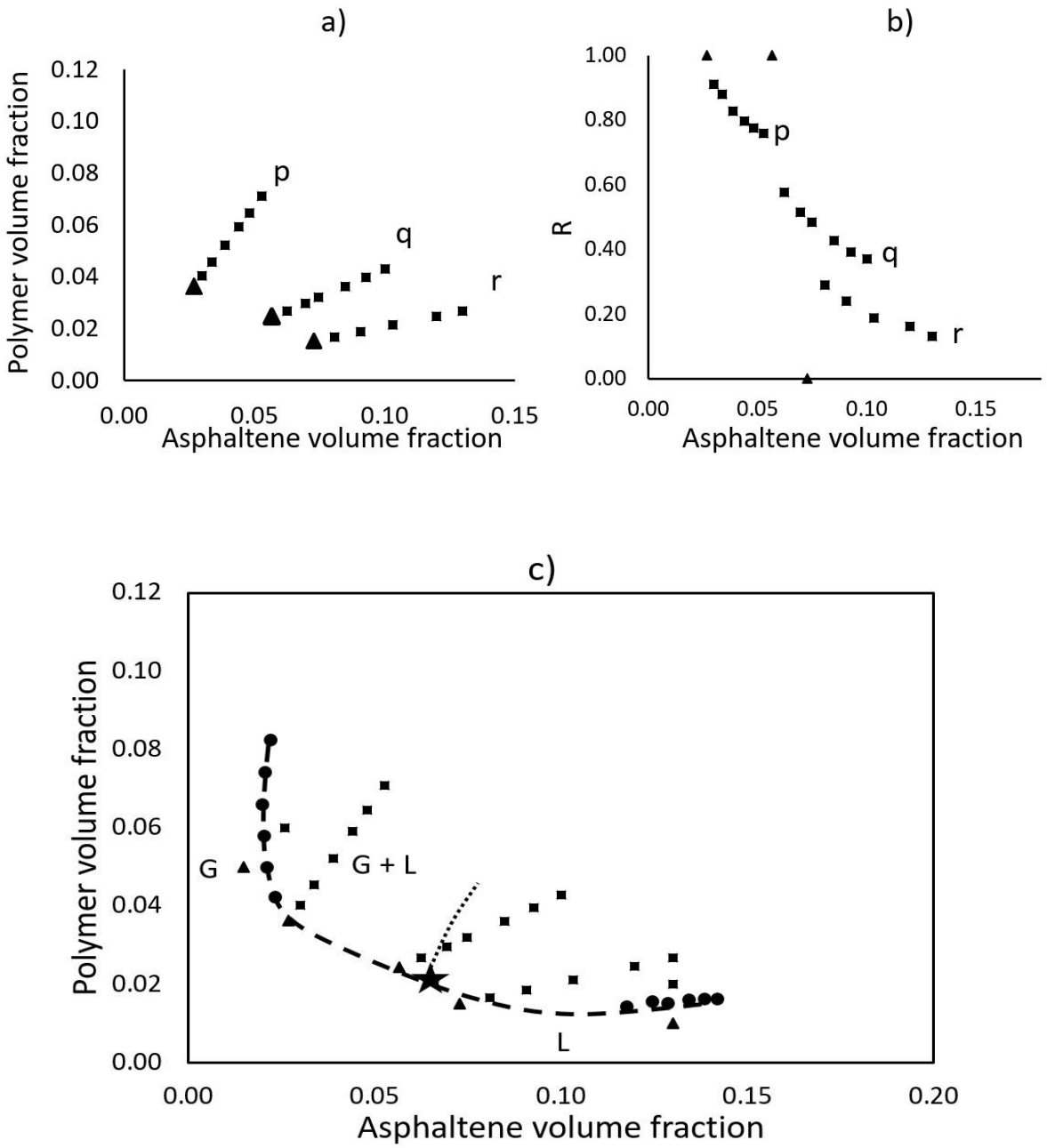

Figure 4.4: Phase behaviour observations (a) along dilution lines p, q and r for mixtures of AB retentate + polystyrene + toluene identified using X-Ray measurements, (b) the volume fraction of the upper phase c) and phase boundary construction details; (■): two-phase; (▲): one-phase; dotted curve: 50 vol% line; (●): binodal points; (★): critical point. Experimental data are reported in Table A.5 and computed points are reported in Table A.6

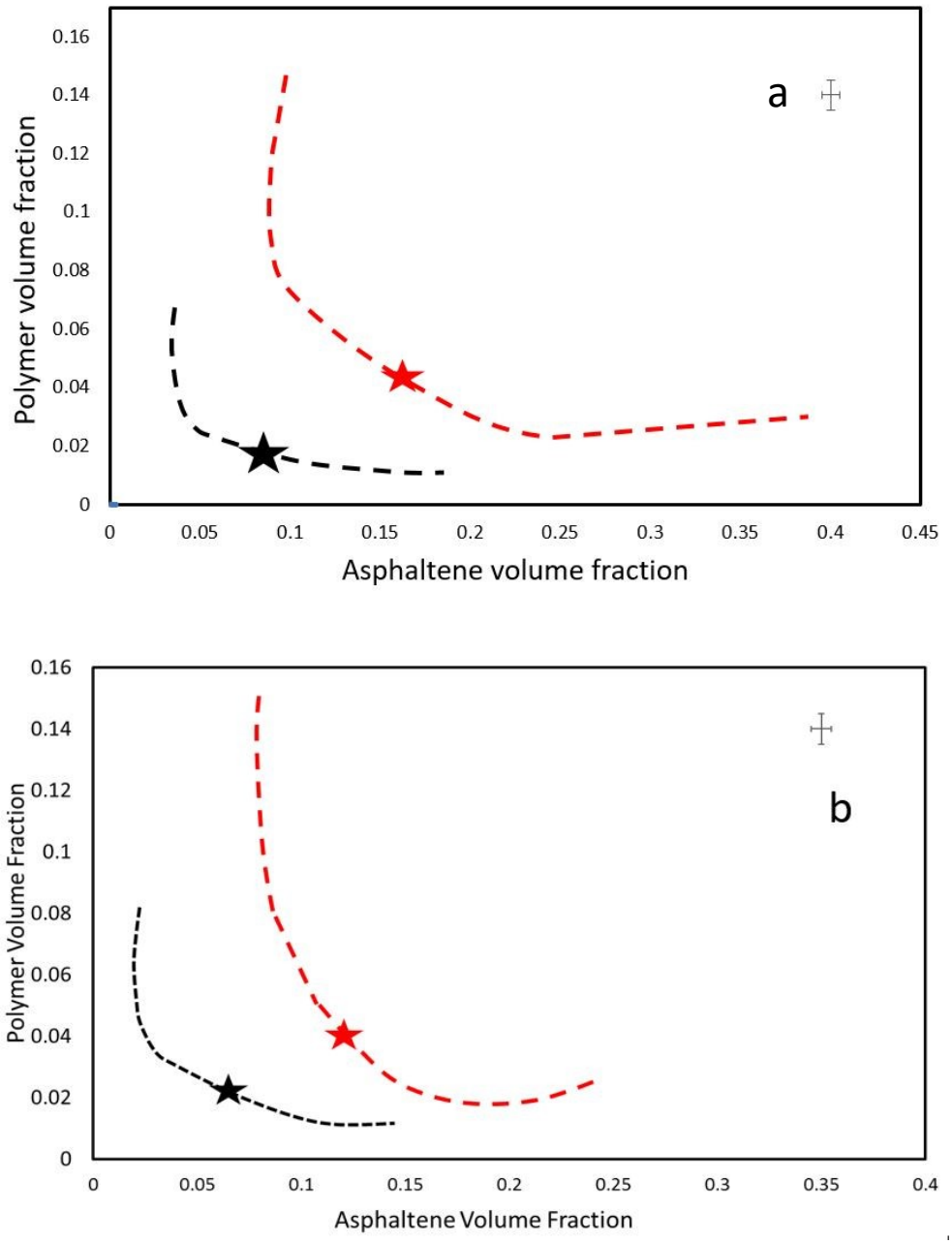

Figure 4.5: Two-phase to one-phase boundary for (a) Athabasca pentane asphaltene + polystyrene + toluene and (b) Athabasca retentate + polystyrene + toluene mixtures measured using acoustic (----) [1] and X-Ray (----) imaging. (★) Critical point measured using acoustic measurements; (★) critical point measured using X-ray transmission.

4.4 Phase Diagrams for Athabasca pentane asphaltenes and asphaltene rich retentate + polystyrene + toluene mixtures

A) At low polymer and nanoparticle volume fractions

At low polymer and nanoparticle mass fractions, the phase diagram construction method of Bodnar [2] provides an efficient way to prepare and compare phase diagrams and to identify critical points. Phase diagrams for retentate + polystyrene + toluene and pentane asphaltene + polystyrene + toluene prepared on this basis are compared in Figure 4.6. The nature and shape of the phase boundaries and the placement of the colloid-liquid colloid-gas critical points L=G are similar. From the relative placement of critical points the average size of the nano-scale particles in the retentate + polystyrene + toluene mixtures is smaller than in asphaltene + polystyrene + toluene mixtures [3]. The acoustic and x-ray methods are consistent in this respect.

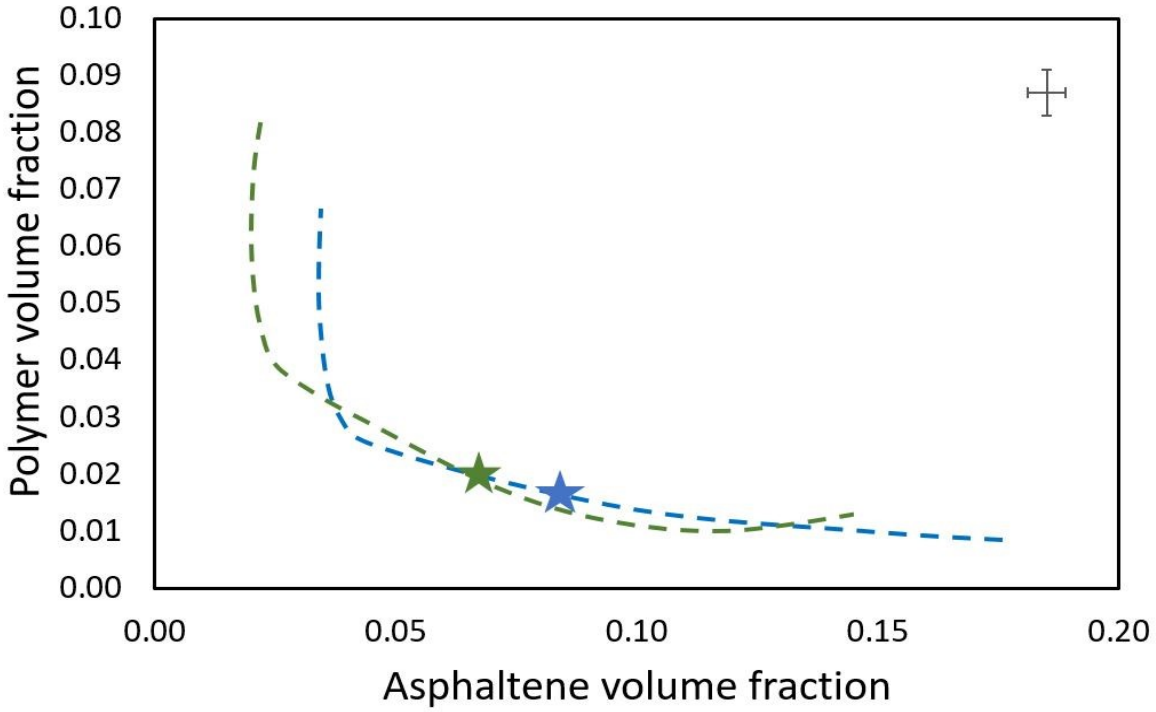

Figure 4.6: Two-phase to one-phase boundary for Athabasca pentane asphaltene + polystyrene + toluene (----) and retentate + polystyrene + toluene (----) mixtures based on x-Ray measurements at low polymer and asphaltene volume fractions. (★) Critical point for pentane asphaltene; (★) critical point for retentate

B) At high polymer and asphaltene volume fractions

When asphaltene is added to polystyrene + toluene mixtures, transitions from single phase colloidal gas (G) or colloid liquid (L) to a two phase L+ G region and then to a single phase G or L region are observed as illustrated by trajectories 1-5 in Figure 4.7. When toluene is added to homogeneous mixtures of asphaltene + polystyrene + toluene, transitions from single phase to two phase G+L behaviour is observed as illustrated by trajectories 6-7 in Figure 4.7. Consequently, the G+L region comprises a closed loop in the phase diagram. This means there should be two

critical points on the G +L to L or G boundary – on corresponding to depletion flocculation and the other corresponding to depletion re-stabilization as illustrated by Kumar [5] in Chapter 2. Critical points were obtained by extrapolating the 50 vol% curve (where G = L = 0.5) to the G+L phase boundary and ensuring that the end point of extrapolations falls between trajectories where R1 = 0 and R1 = 1 at the phase boundary. Critical points and interpolated phase boundary points are shown in Figure 4.8. A qualitatively similar construction for retentate + polystyrene + toluene is shown in Figure 4.9, and Figure 4.10 respectively

Phase diagrams for retentate and asphaltene + polystyrene + toluene mixtures are compared in Figure 4.11. The phase diagrams are qualitatively similar but quantitatively different. The LG two phase region is much smaller for the retentate than for the asphaltenes. However, the two phase boundary and the 50 % curves near the depletion flocculation point (C1) are comparable. The placement of the depletion re-stabilization critical points differs substantially. This difference may be attributable to differences in solvent composition, which are substantial, or to differences in nanoparticle properties. Neither of these topics is resolved in this work or in the prior literature.

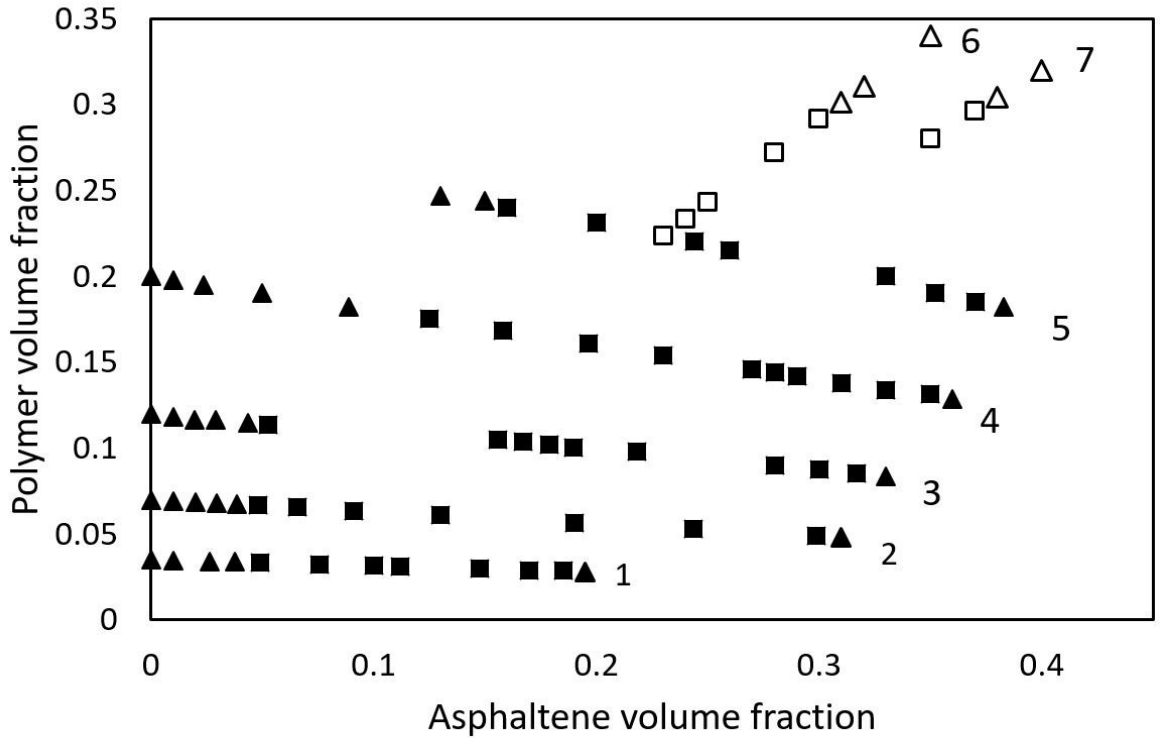

Figure 4.7: Phase behavior observations for pentane asphaltene + polystyrene + toluene mixtures based on X-Ray measurement at 295K. Trajectories are defined in the text. (■, □): two-phase; (▲, △): one-phase; Data are reported in Table A.7.

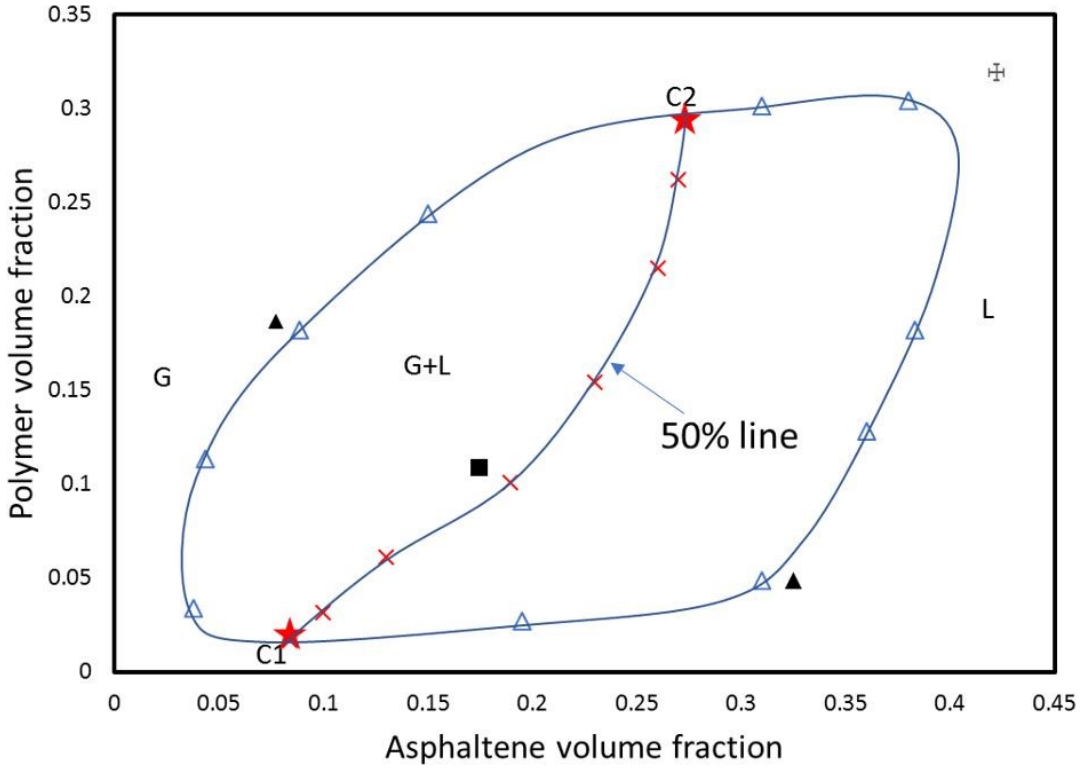

Figure 4.8: Experimental phase diagram for Athabasca pentane asphaltenes + polystyrene + toluene. (G) colloid gas like phase, (L) colloid liquid like phase, (G+L) coexisting colloid liquid like and gas like phases, (△) phase boundary, (x) 0.5 (volume fraction of L and G), (C1) first critical point, and (C2) second critical point, (■) two phase region, (▲) single phase region.

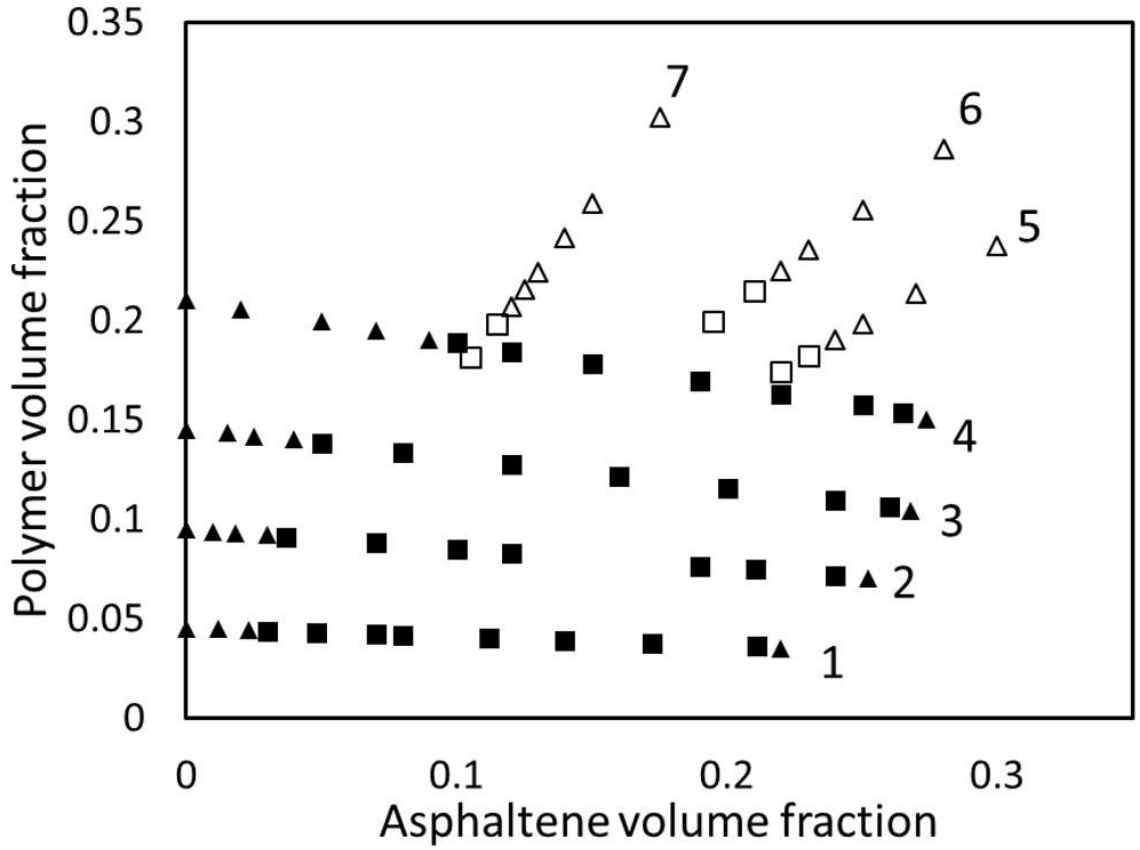

Figure 4.9: Phase behavior observations for retentate + polystyrene + toluene mixtures based on X-ray measurement at 295K. Trajectories are defined in the text. ; (■, □): two-phase; (▲, △): one-phase. Data are reported in Table A.8.

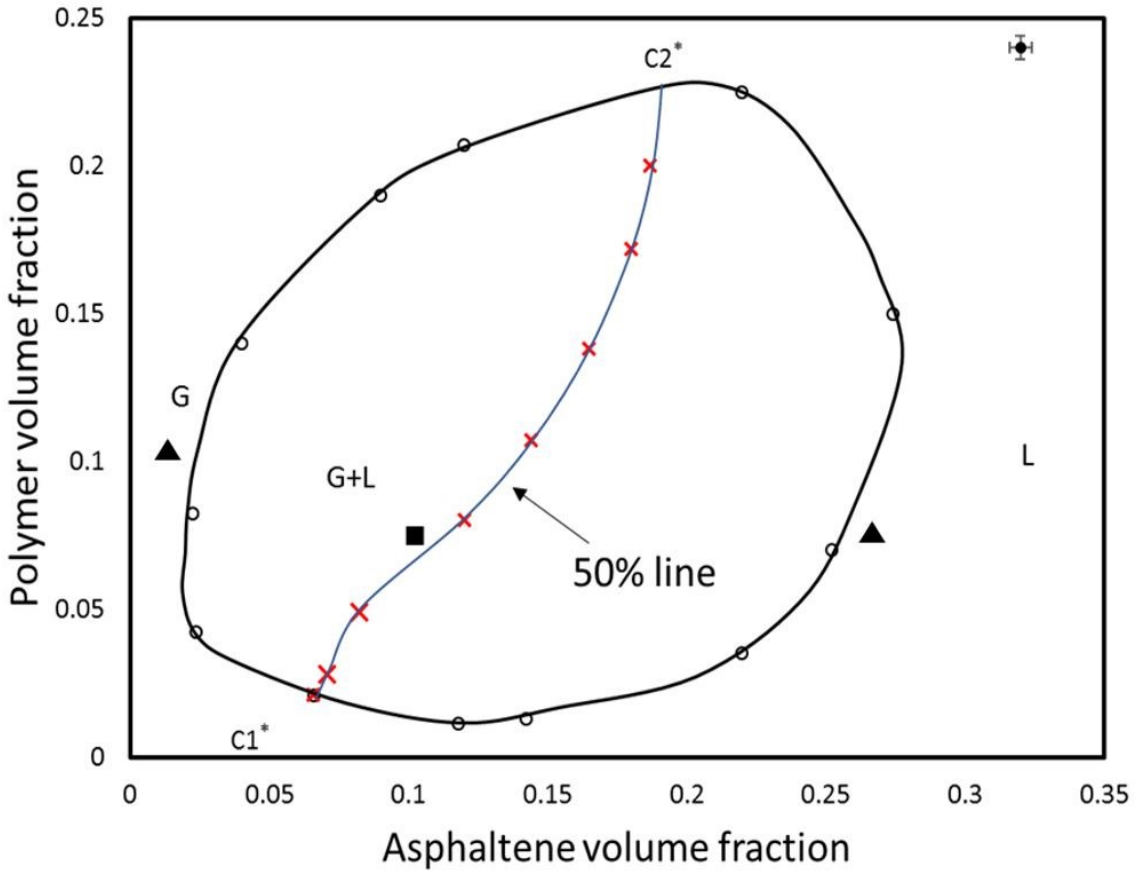

Figure 4.10 Experimental phase diagram for retentate + polystyrene + toluene. (G) colloid gas like phase, (L) colloid liquid like phase, (G+L) coexisting colloid liquid like and gas like phases, (○) phase boundary, (x) 0.5 (volume fraction of L and G), ($C1^*$) first critical point, and ($C2^*$) second critical point, (■) two phase region, (▲) single phase region.

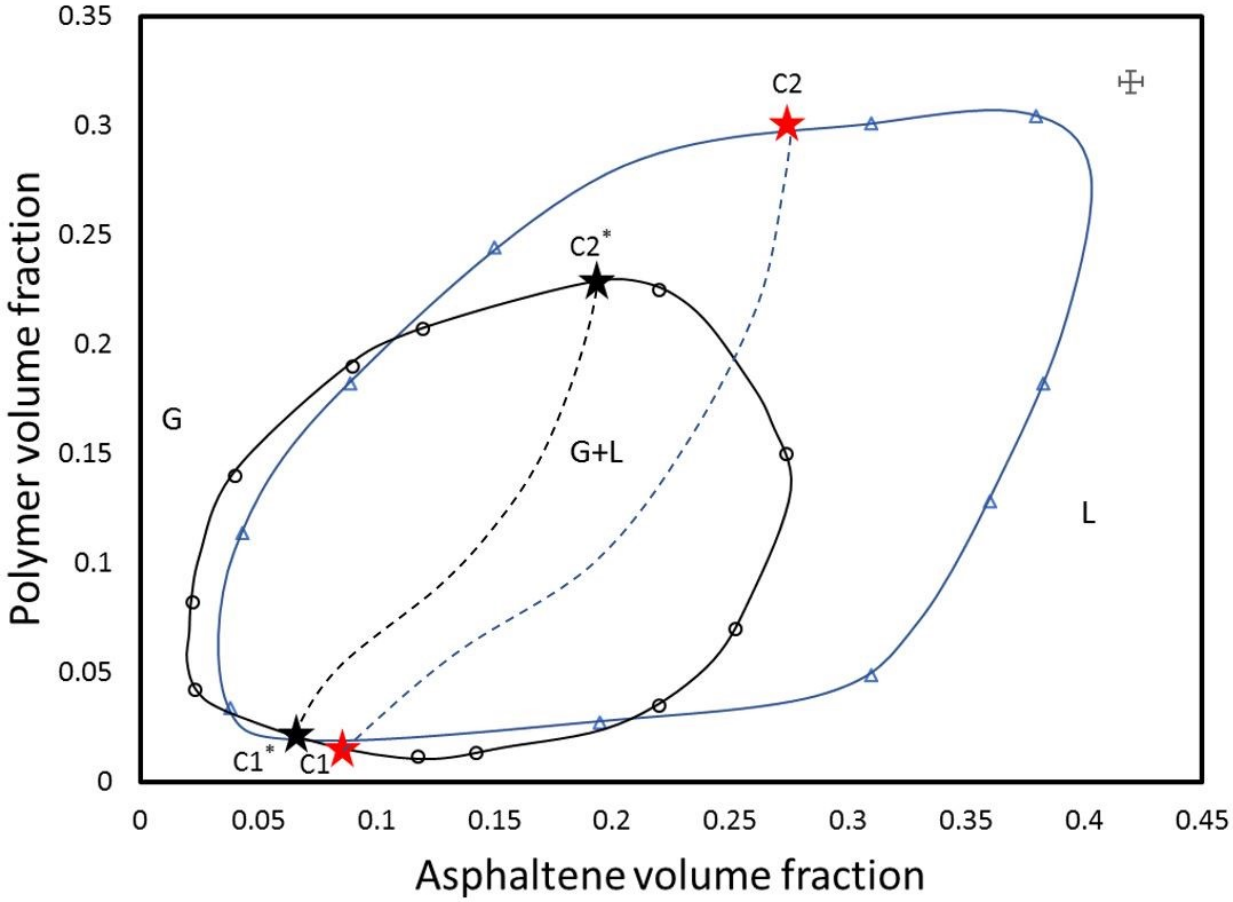

Figure 4.11: Experimental phase diagram of Athabasca Pentane Asphaltenes (blue) and Retentate (black) + toluene + Polystyrene. (△) G+L phase boundary for pentane asphaltene, (○) G+L phase boundary for Retentate (C1, C2) critical points for pentane asphaltene, and (C1*, C2*) critical points for retentate.

References:

1. Pouralhosseini, S., Alizadehgiashi, M., & Shaw, J. M. (2015). On the Phase Behavior of Athabasca Asphaltene+ Polystyrene+ Toluene Mixtures at 298 K. Energy & Fuels, 29(8), 4855-4863.
2. Bodnár, I., & Oosterbaan, W. D. (1997). Indirect determination of the composition of the coexisting phases in a demixed colloid polymer mixture. *The Journal of chemical physics*, *106*(18), 7777-7780.
3. Khammar, M., & Shaw, J. M. (2012). Estimation of phase composition and size of asphaltene colloidal particles in mixtures of asphaltene+ polystyrene+ toluene at 293 K and atmospheric pressure. Fluid Phase Equilibria, 332, 105-119.
4. Dini, Y., Becerra, M., & Shaw, J. M. (2016). Phase Behavior and Thermophysical Properties of Peace River Bitumen + Propane Mixtures from 303 K to 393 K. Journal of Chemical & Engineering Data, 61(8), 2659-2668.
5. Kumar, A. (2018). The Interaction between Depletion Flocculation and Molecular Liquid-Liquid Phase Separation Mechanisms. (MSc thesis, University of Alberta)

Chapter 5: Conclusions and Recommendations

5.1 Conclusions

In this work, the phase behavior of mixtures comprising chemically separated pentane asphaltenes + toluene + atactic polystyrene (400,000 AMU) was revisited and the phase behavior of Athabasca bitumen (naturally-occurring hydrocarbon resource with 18.6 wt.% pentane asphaltenes) + toluene + atactic polystyrene (400,000 AMU) mixtures was explored. For both mixtures critical points associated with depletion flocculation and depletion re-stabilization are identified on closed loop two-phase to one-phase boundaries. This type of phase behaviour was not anticipated from prior work and comprises a significant advance in the understanding of the behaviour of such mixtures.

The experimental methods, phase boundaries, tie lines and fluid-fluid critical points are presented and discussed in detail. X-ray transmission tomography is shown to be more robust than acoustic transmission for the identification of two-phase to one-phase boundaries and critical points in these mixtures. This finding comprises a second significant contribution of the present work.

The outcomes of this work are expected to improve the understanding of asphaltene behaviours in current production, transport, and refining processes, and may lead to a reduction in the failure rate of asphaltene aggregation and deposition models, and the development of new low-environmental impact de-asphalting processes for heavy oils.

5.2 Future Work

- Measure the phase behavior of such mixtures at different temperatures and pressures.
- Measure the nanoparticle mean size and size distribution in both types of mixtures.
- Model the phase behavior of such mixtures to include both the depletion flocculation and re-stabilization effects.
- Test the viability of depletion flocculation/re-stabilization as a basis for de-asphalting process design.
- Test the applicability of the depletion flocculation/re-stabilization as a basis for understanding asphaltene deposition phenomena.

Bibliography

- Abedi, S. J., Cai, H. Y., Seyfaie, S., & Shaw, J. M. (1999). Simultaneous phase behaviour, elemental composition and density measurement using X-ray imaging. *Fluid Phase Equilibria*, *158*, 775-781.
- AlHammadi, A. A., & Chapman, W. G. (2017). Modeling the Polystyrene–Asphaltenes–Toluene Mixture Using the Perturbed-Chain Form of Statistical Associating Fluid Theory Equation of State. *Energy & Fuels*, *31*(6), 6019-6024.
- Amundaraín Hurtado, J. L., Chodakowski, M., Long, B., & Shaw, J. M. (2011). Characterization of physically and chemically separated Athabasca asphaltenes using small-angle X-ray scattering. *Energy & Fuels*, *25*(11), 5100-5112.
- Anderson, V. J., & Lekkerkerker, H. N. (2002). Insights into phase transition kinetics from colloid science. Nature, 416(6883), 811.
- Antl, L., Goodwin, J. W., Hill, R. D., Ottewill, R. H., Owens, S. M., Papworth, S., & Waters, J. A. (1986). The preparation of poly (methyl methacrylate) latices in non-aqueous media. Colloids and Surfaces, 17(1), 67-78.
- Asakura, S., & Oosawa, F. (1954). On interaction between two bodies immersed in a solution of macromolecules. *The Journal of Chemical Physics*, *22*(7), 1255-1256.
- Barré, L., Simon, S., & Palermo, T. (2008). Solution properties of asphaltenes. *Langmuir*, *24*(8), 3709-3717.
- Bodnár, I., & Oosterbaan, W. D. (1997). Indirect determination of the composition of the coexisting phases in a demixed colloid polymer mixture. *The Journal of chemical physics*, *106*(18), 7777-7780.

- Chávez-Miyauchi, T. E., Zamudio-Rivera, L. S., & Barba-López, V. (2013). Aromatic polyisobutylene succinimides as viscosity reducers with asphaltene dispersion capability for heavy and extra-heavy crude oils. *Energy & Fuels*, *27*(4), 1994-2001.
- Chang, C. L., & Fogler, H. S. (1994). Stabilization of asphaltenes in aliphatic solvents using alkylbenzene-derived amphiphiles. 1. Effect of the chemical structure of amphiphiles on asphaltene stabilization. *Langmuir*, *10*(6), 1749-1757.
- Ching, M. J. T. M., Pomerantz, A. E., Andrews, A. B., Dryden, P., Schroeder, R., Mullins, O. C., & Harrison, C. (2010). On the nanofiltration of asphaltene solutions, crude oils, and emulsions. *Energy & Fuels*, *24*(9), 5028-5037.
- Crocker, J. C., Matteo, J. A., Dinsmore, A. D., & Yodh, A. G. (1999). Entropic attraction and repulsion in binary colloids probed with a line optical tweezer. Physical review letters, 82(21), 4352
- De Boer, R. B., Leerlooyer, K., Eigner, M. R. P., & Van Bergen, A. R. D. (1995). Screening of crude oils for asphalt precipitation: theory, practice, and the selection of inhibitors. SPE Production & Facilities, 10(01), 55-61.
- Dickinson, E., & Eriksson, L. (1991). Particle flocculation by adsorbing polymers. Advances in Colloid and Interface Science, 34, 1-29.
- Dini, Y., Becerra, M., & Shaw, J. M. (2016). Phase Behavior and Thermophysical Properties of Peace River Bitumen+ Propane Mixtures from 303 K to 393 K. Journal of Chemical & Engineering Data, 61(8), 2659-2668.
- Dwiggins, C. W. (1978). Study of colloidal nature of petroleum with an automated Bonse–Hart X-ray small-angle scattering unit. *Journal of Applied Crystallography*, *11*(5), 615-619.

- Espinat, D., Fenistein, D., Barre, L., Frot, D., & Briolant, Y. (2004). Effects of temperature and pressure on asphaltenes agglomeration in toluene. A light, X-ray, and neutron scattering investigation. *Energy & fuels*, *18*(5), 1243-1249.
- Eyssautier, J., Espinat, D., Gummel, J., Levitz, P., Becerra, M., Shaw, J., & Barré, L. (2011). Mesoscale organization in a physically separated vacuum residue: comparison to asphaltenes in a simple solvent. Energy & Fuels, 26(5), 2680-2687.
- Fernández, L., Sigal, E., Otero, L., Silber, J. J., & Santo, M. (2011). Solubility improvement of an anthelmintic benzimidazole carbamate by association with dendrimers. Brazilian Journal of Chemical Engineering, 28(4), 679-689.
- Fleer, G. J., & Tuinier, R. (2008). Analytical phase diagrams for colloids and non-adsorbing polymer. *Advances in colloid and interface science*, *143*(1), 1-47.
- Fleer, G. J., & Scheutjens, J. M. H. M. (1987). Effect of adsorbing and nonadsorbing polymer on the interaction between colloidal particles. *Croatica Chemica Acta*, *60*(3), 477-494.
- Gast, A. P., Hall, C. K., & Russel, W. B. (1983). Polymer-induced phase separations in nonaqueous colloidal suspensions. *Journal of Colloid and Interface Science*, *96*(1), 251-267.
- Gast, A. P., Russel, W. B., & Hall, C. K. (1986). An experimental and theoretical study of phase transitions in the polystyrene latex and hydroxyethylcellulose system. *Journal of colloid and interface science*, *109*(1), 161-171.
- Hashmi, S. M., Quintiliano, L. A., & Firoozabadi, A. (2010). Polymeric dispersants delay sedimentation in colloidal asphaltene suspensions. *Langmuir*, *26*(11), 8021-8029.
- Hiemenz, P. C., & Rajagopalan, R. (Eds.). (1997). *Principles of Colloid and Surface Chemistry, revised and expanded* (Vol. 14). CRC press.

- Hunter, R. J. (1993). *Introduction to modern colloid science*. Oxford University Press.
- Jenkins, P., & Snowden, M. (1996). Depletion flocculation in colloidal dispersions. *Advances in colloid and interface science*, *68*, 57-96.
- Kabel, K. I., Abdelghaffar, A. M., Farag, R. K., Maysour, N. E., & Zahran, M. A. (2015). Synthesis and evaluation of PAMAM dendrimer and PDPF-b-POP block copolymer as asphaltene inhibitor/dispersant. *Research on Chemical Intermediates*, *41*(1), 457-474.
- Khammar, M., & Shaw, J. M. (2011). Phase behaviour and phase separation kinetics measurement using acoustic arrays. *Review of Scientific Instruments*, *82*(10), 104902.
- Khammar, M., & Shaw, J. M. (2012). Estimation of phase composition and size of asphaltene colloidal particles in mixtures of asphaltene+ polystyrene+ toluene at 293 K and atmospheric pressure. Fluid Phase Equilibria, 332, 105-119.
- Khammar, M., & Shaw, J. M. (2011). Liquid–liquid phase equilibria in asphaltene+ polystyrene+ toluene mixtures at 293 K. *Energy & Fuels*, *26*(2), 1075-1088.
- Kim, S., Hyun, K., Moon, J. Y., Clasen, C., & Ahn, K. H. (2015). Depletion stabilization in nanoparticle–polymer suspensions: multi-length-scale analysis of microstructure. Langmuir, 31(6), 1892-1900.
- Kumar, A. (2018). The Interaction between Depletion Flocculation and Molecular Liquid-Liquid Phase Separation Mechanisms. (MSc thesis, University of Alberta)
- Kumar, A. & Shaw, J. M. (2018). Combining Depletion Re-stabilization and Depletion Flocculation Effects in Phase Diagrams for Colloid + Polymer Mixtures (in preparation).
- Lekkerkerker, H. N. W., Poon, W. K., Pusey, P. N., Stroobants, A., & Warren, P. 0. (1992). Phase behaviour of colloid+ polymer mixtures. *EPL (Europhysics Letters)*, *20*(6), 559.

- Lima, A. F., Mansur, C. R., Lucas, E. F., & González, G. (2010). Polycardanol or sulfonated polystyrene as flocculants for asphaltene dispersions. *Energy & Fuels*, *24*(4), 2369-2375.
- Mao, Y., Cates, M. E., & Lekkerkerker, H. N. W. (1995). Depletion force in colloidal systems. Physica A: Statistical Mechanics and its Applications, 222(1-4), 10-24.
- McKenna, A. M., Blakney, G. T., Xian, F., Glaser, P. B., Rodgers, R. P., & Marshall, A. G. (2010). Heavy petroleum composition. 2. Progression of the Boduszynski model to the limit of distillation by ultrahigh-resolution FT-ICR mass spectrometry. Energy & Fuels, 24(5), 2939-2946.
- Mostowfi, F., Indo, K., Mullins, O. C., & McFarlane, R. (2008). Asphaltene nanoaggregates studied by centrifugation. *Energy & fuels*, *23*(3), 1194-1200.
- Maham, Y., Chodakowski, M. G., Zhang, X., & Shaw, J. M. (2005). Asphaltene phase behavior: prediction at a crossroads. Fluid Phase Equilibria, 228, 21-26.
- Murray, B. S., & Phisarnchananan, N. (2014). The effect of nanoparticles on the phase separation of waxy corn starch+ locust bean gum or guar gum. *Food Hydrocolloids*, *42*, 92-99.
- Mullins, O. C., Sheu, E. Y., Hammami, A., & Marshall, A. G. (2007). *Asphaltenes, heavy oils, and petroleomics*. Springer Science & Business Media.
- Oilfieldwiki.com. (2018). File:Deboer.jpg - OilfieldWiki. [online] Available at: http://www.oilfieldwiki.com/wiki/File:Deboer.jpg [Accessed 3 May 2018].
- Overfield, R. E., Sheu, E. Y., Sinha, S. K., & Liang, K. S. (1989). SANS study of asphaltene aggregation. *Fuel science & technology international*, *7*(5-6), 611-624.
- Poon, W. C. K. (2002). The physics of a model colloid–polymer mixture. Journal of Physics: Condensed Matter, 14(33), R859.

- Pouralhosseini, S., Alizadehgiashi, M., & Shaw, J. M. (2015). On the Phase Behavior of Athabasca Asphaltene+ Polystyrene+ Toluene Mixtures at 298 K. Energy & Fuels, 29(8), 4855-4863.
- Pouralhosseini, S., Eslami, F., Elliott, J. A., & Shaw, J. M. (2016). Modeling the Phase Behavior of Asphaltene+ Toluene+ Polystyrene Mixtures A Depletion Flocculation Approach. *Energy & Fuels*, *30*(2), 904-914.
- Russel, W. B., Saville, D. A., & Schowalter, W. R. (1989). *Colloidal dispersions*. Cambridge university press.
- Semenov, A. N. (2008). Theory of colloid stabilization in semidilute polymer solutions. Macromolecules, 41(6), 2243-2249.
- Sheu, E. Y., Storm, D. A., & Maureen, M. (1991). Asphaltenes in polar solvents. *Journal of non-crystalline solids*, *131*, 341-347.
- Sheu, E. Y. (2006). Small angle scattering and asphaltenes. Journal of Physics: Condensed Matter, 18(36), S2485.
- Sieglaff, C. L. (1959). Phase separation in mixed polymer solutions. *Journal of Polymer Science Part A: Polymer Chemistry*, *41*(138), 319-326.
- Speight, J. G., & Moschopedis, S. E. (1981). On the molecular nature of petroleum asphaltenes.
- Tanaka, S., & Ataka, M. (2002). Protein crystallization induced by polyethylene glycol: A model study using apoferritin. *The Journal of chemical physics*, *117*(7), 3504-3510.
- Tuinier, R., Smith, P. A., Poon, W. C. K., Egelhaaf, S. U., Aarts, D. G. A. L., Lekkerkerker, H. N. W., & Fleer, G. J. (2008). Phase diagram for a mixture of colloids and polymers with equal size. *EPL (Europhysics Letters)*, *82*(6), 68002.

- Vincent, B., Edwards, J., Emmett, S., & Croot, R. (1988). Phase separation in dispersions of weakly-interacting particles in solutions of non-adsorbing polymer. *Colloids and Surfaces*, *31*, 267-298.
- Walz, J. Y., & Sharma, A. (1994). Effect of long range interactions on the depletion force between colloidal particles. Journal of colloid and interface science, 168(2), 485-496.
- Zhao, B., & Shaw, J. M. (2007). Composition and size distribution of coherent nanostructures in Athabasca bitumen and Maya crude oil. Energy & Fuels, 21(5), 2795-2804.

Appendix: Experimental Data

Table A.1: Compositions and associated polymer-rich phase volume data for retentate + polystyrene + toluene (based on speed of sound measurements) for trajectories p, q, and r (Figure 4.1a and 4.1 b)

	Asphaltene volume fraction	Polystyrene volume fraction	Volume fraction of the upper phase (R)
p	0.128	0.116	0.690
	0.121	0.110	0.704
	0.114	0.104	0.730
	0.107	0.097	0.753
	0.100	0.091	0.818
	0.093	0.085	0.880
q	0.155	0.073	0.432
	0.148	0.070	0.441
	0.141	0.067	0.456
	0.134	0.063	0.471
	0.127	0.060	0.511
	0.120	0.057	0.560
r	0.173	0.052	0.270
	0.166	0.050	0.270
	0.159	0.048	0.280
	0.152	0.046	0.290
	0.145	0.044	0.300
	0.138	0.041	0.320
	0.131	0.039	0.330

Table A.2: Computed binodal points for retentate + polystyrene + toluene based on speed of sound measurements (Figure 4.1 c)

Asphaltene volume fraction	Polystyrene volume fraction
0.082	0.097
0.080	0.109
0.079	0.121
0.079	0.132
0.079	0.143
0.080	0.151
0.174	0.020
0.186	0.022
0.195	0.021
0.205	0.022
0.218	0.022
0.238	0.028

Table A.3: Compositions and associated polymer-rich phase volume data for pentane asphaltene + polystyrene + toluene (based on X-Ray measurements) for trajectories p, q, and r (Figure 4.3a and 4.3b)

	Asphaltene volume fraction	Polystyrene volume fraction	Volume fraction of the upper phase (R)
p	0.065	0.042	0.754
	0.059	0.039	0.797
	0.055	0.035	0.850
	0.050	0.033	0.896
	0.047	0.030	0.930
	0.044	0.028	0.956
q	0.103	0.030	0.464
	0.094	0.028	0.505
	0.086	0.025	0.553
	0.079	0.023	0.615
	0.074	0.022	0.650
	0.069	0.020	0.689
r	0.130	0.024	0.282
	0.119	0.022	0.313
	0.110	0.020	0.346
	0.100	0.018	0.370
	0.094	0.017	0.393
	0.088	0.016	0.422

Table A.4: Computed binodal points for pentane asphaltene + polystyrene + toluene based on X-ray measurements (Figure 4.3c)

Asphaltene volume fraction	Polystyrene volume fraction
0.039	0.028
0.038	0.035
0.036	0.042
0.036	0.050
0.034	0.058
0.035	0.066
0.138	0.013
0.144	0.012
0.153	0.011
0.158	0.010
0.168	0.010
0.176	0.010

Table A.5: Compositions and associated polymer-rich phase volume data for retentate + polystyrene + toluene (based on X-Ray measurements) for trajectories p, q, and r (Figure 4.4a and 4.4b)

	Asphaltene volume fraction	Polystyrene volume fraction	Volume fraction of the upper phase (R)
p	0.053	0.071	0.760
	0.048	0.064	0.775
	0.044	0.059	0.798
	0.039	0.052	0.829
	0.034	0.045	0.880
	0.030	0.040	0.911
q	0.100	0.043	0.371
	0.093	0.040	0.393
	0.085	0.036	0.427
	0.075	0.032	0.484
	0.070	0.030	0.517
	0.063	0.027	0.576
r	0.13	0.03	0.13
	0.12	0.02	0.16
	0.10	0.02	0.19
	0.09	0.02	0.24
	0.08	0.02	0.29

Table A.6: Computed binodal points for retentate + polystyrene + toluene based on X-ray measurements (Figure 4.4c)

Asphaltene volume fraction	Polystyrene volume fraction
0.118	0.011
0.125	0.013
0.129	0.012
0.135	0.013
0.139	0.013
0.142	0.013
0.023	0.042
0.021	0.050
0.021	0.058
0.020	0.066
0.021	0.074
0.022	0.082

Table A.7: Compositions and associated polymer-rich phase volume data for pentane asphaltene + polystyrene + toluene (based on X-Ray measurements) for trajectories 1, 2, 3, 4, 5, 6, 7 (Figure 4.7)

1		
Asphaltene volume fraction	polymer volume fraction	R(upper phase volume fraction)
0.040	0.034	0.900
0.049	0.033	0.820
0.076	0.032	0.650
0.100	0.032	0.500
0.112	0.031	0.440
0.148	0.030	0.310
0.170	0.029	0.170
0.185	0.029	0.100

2		
Asphaltene volume fraction	Polymer volume fraction	R (upper phase volume fraction)
0.048	0.067	0.860
0.066	0.065	0.700
0.091	0.064	0.590
0.130	0.061	0.490
0.190	0.057	0.320
0.243	0.053	0.200
0.299	0.049	0.150

3		
Asphaltene volume fraction	Polymer volume fraction	R (upper phase volume fraction)
0.053	0.114	0.870
0.156	0.105	0.590
0.167	0.104	0.557
0.179	0.102	0.520
0.218	0.098	0.440
0.280	0.090	0.280
0.300	0.088	0.180
0.190	0.101	0.500
0.317	0.085	0.130

4		
Asphaltene volume fraction	Polymer volume fraction	R (upper phase volume fraction)
0.125	0.175	0.840
0.158	0.168	0.690
0.196	0.161	0.580
0.270	0.146	0.380
0.230	0.154	0.500
0.280	0.144	0.350
0.290	0.142	0.310
0.310	0.138	0.240
0.330	0.134	0.180

5		
Asphaltene volume fraction	Polymer volume fraction	R (upper phase volume fraction)
0.160	0.240	0.850
0.200	0.231	0.700
0.244	0.220	0.546
0.260	0.215	0.510
0.330	0.200	0.320
0.352	0.190	0.230
0.370	0.185	0.160

6		
Asphaltene volume fraction	Polymer volume fraction	R (upper phase volume fraction)
0.300	0.291	0.460
0.280	0.272	0.480
0.250	0.243	0.540
0.240	0.233	0.570
0.230	0.223	0.590

Table A.8: Compositions and associated polymer-rich phase volume data for retentate + polystyrene + toluene (based on X-Ray measurements) for trajectories 1, 2, 3, 4, 5, 6, 7 (Figure 4.9)

1		
Asphaltene volume fraction	polymer volume fraction	R(upper phase volume fraction)
0.030	0.044	0.850
0.048	0.043	0.670
0.070	0.042	0.530
0.080	0.041	0.470
0.112	0.040	0.390
0.140	0.039	0.330
0.172	0.037	0.290
0.211	0.036	0.160

2		
Asphaltene volume fraction	Polymer volume fraction	R (upper phase volume fraction)
0.037	0.091	0.850
0.070	0.088	0.680
0.100	0.085	0.570
0.120	0.083	0.500
0.190	0.076	0.280
0.211	0.075	0.200
0.240	0.071	0.130

3		
Asphaltene volume fraction	Polymer volume fraction	R (upper phase volume fraction)
0.050	0.138	0.880
0.080	0.133	0.730
0.120	0.127	0.580
0.160	0.121	0.460
0.200	0.115	0.320
0.240	0.109	0.200
0.260	0.106	0.140

4		
Asphaltene volume fraction	Polymer volume fraction	R (upper phase volume fraction)
0.100	0.188	0.920
0.120	0.184	0.810
0.150	0.178	0.670
0.190	0.169	0.460
0.220	0.163	0.320
0.250	0.158	0.160
0.265	0.153	0.100

5		
Asphaltene volume fraction	Polymer volume fraction	R (upper phase volume fraction)
0.230	0.182	0.310
0.220	0.174	0.290

6		
Asphaltene volume fraction	Polymer volume fraction	R (upper phase volume fraction)
0.210	0.215	0.470
0.195	0.199	0.440

7		
Asphaltene volume fraction	Polymer volume fraction	R (upper phase volume fraction)
0.115	0.198	0.800
0.105	0.181	0.840